The use of tailormade 3D-printed shoes in horses

Comparing kinetic parameters, hoof conformation and wear characteristics of the shoe in horses wearing steel shoes and tailormade 3D-printed plastic shoes

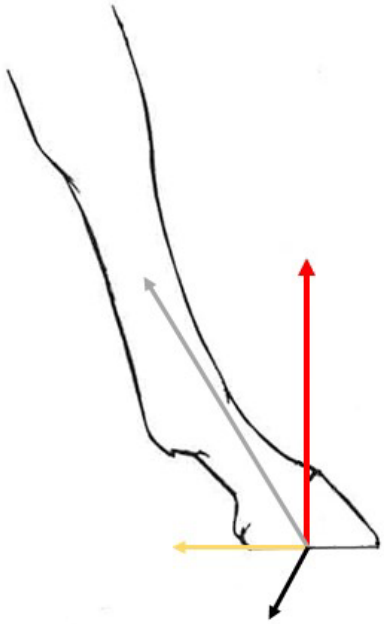

Merel Charlotte Hartmann

4248007

m.c.hartmann@students.uu.nl

Veterinary Medicine Master Thesis, Utrecht University

Supervisor

J.I.M. Parmentier[1,2]

[1]Faculty of Veterinary Medicine, Department of Clinical Sciences, Utrecht University, The Netherlands

[2]EEMCS, Pervasive Systems Group, University of Twente, Enschede, The Netherlands

Abstract

Researchers of the University of Utrecht recently introduced a tailormade three-dimensional (3D) printed shoe. The aim of this study is to investigate the effects of this 3D-printed shoe on kinetic parameters, hoof conformation and to investigate its wear characteristics. The shoes were designed based on a 3D scan of the hoof, printed in plastic materials, and then glued to the hooves. Six horses underwent a 3D-printed shoeing cycle and a steel shoeing cycle of seven weeks in randomised order. Kinetic parameters were collected in trot using pressure- and force plates at a frequency of 250 Hz at week 1 (T0) and week 7 (T1). Hoof pictures were taken at T0 and T1 to determine the hoof conformation and wear characterises of the shoes. Data were analysed using a linear mixed effect model with shoeing conditions and timepoints as fixed effects and horse and limbs as random effects. The results showed a significantly larger peak vertical force (PVF) and vertical impulse (VI) at both timepoints in the 3D-printed shoes (T0: +0.9 N/kg; *p value* = .001 and +179.0 N.s/kg; *p value* = .005, T1: +1.3 N/kg; *p value* < .001 and +294.7 N.s/kg; *p value* < .001). The peak pressure was more evenly distributed between the regions of the hoof in the 3D-printed shoes at both timepoints. The hoof conformation variables indicate a more balanced hoof growth (and/or wear) in the 3D-printed shoeing cycle. The wear distribution of the 3D-printed shoes was more homogenous. The higher PVF and VI values in the 3D-printed shoes suggest that horses exerted more force on the concerning limb. The homogenous wear distribution in the 3D-printed shoes could be explained by the evenly distributed peak pressure in tailormade 3D-printed shoes.

Keywords: horses, horseshoes, steel shoes, tailormade 3D-printed shoes, kinetics, force plate, pressure plate, hoof conformation, wear

Table of Contents

Preface

The curriculum of the study Veterinary Medicine at the University of Utrecht includes a research project in the master programme equine health. This master thesis is the final report of the research project carried out by M. C. Hartmann under supervision of J.I.M. Parmentier. The research project took place at the Department of Clinical Sciences of the University of Utrecht.

Research was conducted to investigate the use of tailormade 3D-printed shoes in horses. Six rider-sound horses were shod with the tailormade 3D-printed shoes and steel shoes to compare the effects on kinematic and kinetic parameters, hoof conformation and wear of the shoes. The kinematic data will be analysed in another master thesis. This paper describes the effects of tailormade 3D-printed shoes on kinetics, hoof conformation and wear of the shoes.

I would like to thank my supervisor, Jeanne Parmentier, for her guidance during this project. Furthermore, I am grateful to have participated in the research team concerning the 3D-printed shoes and thus I would like to thank Harold Brommer, Jan de Zwaan, Gerben Bronkhorst and all the other people who were involved in this research.

Lists of abbreviations, figures and tables

Abbreviations

FP: force plate
GRF: ground reaction forces
GRFx: longitudinal ground reaction force
GRFy: transverse ground reaction force
GRFz: vertical ground reaction force
PP: pressure plate
PVF: peak vertical force
StDur: stance duration
tPVF: time to peak vertical force
VI: vertical impulse

Figures

Tables

Introduction

The primary reason to shoe horses has been -and still is- to prevent and protect the hooves from excessive wear (Roepstorff et al., 1999). As empirical knowledge increased, farriers and veterinarians gave new functions to the horseshoe; to improve the performance and welfare of the horse. The hooves play an important role in the locomotion of the horse since an imbalance of the hooves can lead to lameness (Wiggers et al., 2015). Through trimming and shoeing, deviations in the hoof conformation can be minimalised.

Orthopaedic shoeing can be a useful aid in the recovery of disorders in the musculoskeletal system (Oosterlinck et al., 2017). By modifying the surface of contact or pressure distribution under the hoof, it has become possible to relieve specific traumatised structures in the limb and hooves of the horse. However, some horses cannot be helped with the orthopaedic shoes that are currently on the market. For these cases, a personalised solution would be of high interest.

Since the introduction of the steel shoe, two thousand years ago, different types of materials and shapes made their introduction in the farrier field (Back & Pille, 2013). Examples of these are steel egg bar shoes, plastic glue-on-frog-supportive shoes and wooden clogs.

Improved technology has given rise to new measurement instruments to evaluate the hoof balance and pressure distribution (Oosterlinck et al., 2017). This development has given insight to the already existing shoeing techniques. Moreover, the new measurement instruments used in scientific research led to further science-based development of new shoes and a better understanding of equine locomotion.

Recently a group of University of Utrecht researchers, including farriers, vets and engineers introduced the idea of tailormade 3D-printed horseshoes made of a special plastic composition. By scanning the hooves with a 3D-scanner, a horseshoe that fits the conformation of the individual hoof can be produced. In addition, orthopaedic changes can be made to the shoe through a software program. This would enable a totally personalised therapeutic design for the individual horse. Research to investigate the effects of the tailormade 3D-printed shoes in horses needs to be done before the shoes can be applied in clinical patients and/or to put the shoes on the market.

Six horses from the University of Utrecht were used in this research. Kinetic measurements were conducted over one tailormade 3D-printed shoeing cycle and two steel shoeing cycles. This master thesis will describe the effects of the tailormade 3D-printed shoes on kinetic parameters in the stance phase, hoof conformation and wear of the shoes compared to steel shoes. Background information on anatomical planes and rotations, gait biomechanics, kinetics, biomechanics of the hoof, and horseshoes can be found in the Supplement, which is attached at the end of this master thesis.

The following hypothesis were tested:

H0.1 = there is no significant difference between the shoeing conditions and between timepoints in ground reaction forces.

H1.1 = there is a significant difference between the shoeing conditions and between timepoints in the ground reaction forces.

The peak vertical ground reaction force depends on the horse its speed, body mass and how much force the horse puts on the concerning limb. If a difference is found between the shoeing conditions or

timepoints while the speed and weight of the horse remain the same, it means that the horse modifies the force exerted by the limb.

H0.2 = there is no significant difference between the shoeing conditions and between timepoints in pressure distribution.

H1.2 = there is a significant difference between the shoeing conditions and between timepoints in the pressure distribution.

As the tailormade 3D-printed shoes have a different shape than the steel shoes, especially concerning frog- and heel support, the contact area under the heel region of the hoof is larger. Therefore, the tailormade 3D-printed shoes will have an altered pressure distribution compared to the steel shoes.

H0.3 = there is no significant difference between the shoeing conditions in hoof conformation.

H1.3 = there is a significant difference between the shoeing conditions in the hoof conformation.

The tailormade 3D-printed shoes and the steel shoes are not known to affect the hoof growth and thus hoof conformation. Hoof growth is mainly linked to nutrition however, balanced hooves could support hoof growth.

H0.4 = there is no significant difference between the shoeing conditions in wear of the shoes.

H1.4 = there is a significant difference between the shoeing conditions in wear of the shoes.

Due to the lower corrosion resistance of plastic in comparison to steel, the tailormade 3D-printed shoe is likely to wear more than the steel shoe.

I. Materials and methods

1. Horses

Six rider-sound horses were included in this study (mean age 13 ± 2 years, bodyweight 581 ± 37 kg, wither height 161 ± 4 cm, calculated from table 11 in the appendix). All horses were part of the herd of teaching horses of Utrecht University and were regularly used for education and pleasure riding by the student riding school. This research project was approved by the local ethics committee in compliance with the Dutch Act on Animal Experimentation (project no. (AKROP/AVD) 10801-2020-07).

2. Shoeing regime

The horses were first divided into three groups, each consisting of two individuals. These pairs followed three shoeing cycles of 7 weeks in randomised order including two cycles with the steel shoes and one cycle with the tailormade 3D-printed shoes, as seen in table 1. The farriers knew which type of shoes they were going to apply to which horse and the researchers knew which shoes were applied to which horse during the measurements. The data from the measurements of the first steel shoeing cycle was not analysed in this research paper due to missing data as the pressure-force plate system was unavailable.

Horse	**1st shoeing cycle**	**2nd shoeing cycle**	**3rd shoeing cycle**
H1, H2	3D-printed shoes	Steel shoes	Steel shoes
H3, H4	Steel shoes	3D-printed shoes	Steel shoes
H5, H6	Steel shoes	Steel shoes	3D-printed shoes

Table 1: overview of the shoeing cycles per horse pair.

The tailormade 3D-printed horseshoes, shown in figure 1, were developed by the department of clinical science at the University of Utrecht. The shoes are made up of Hytrel® from the brand DuPon, which is a thermoplastic elastomer, with a 12 mm thick sole, frog support and the shoes cover part of the outer

hoof wall. The weight of the shoes was 224.3 ± 24 gr. The sole of the shoes was printed in two colours changing every 1 mm to monitor the wear of the shoes.

Figure 1: the lateral and solar view of the left front hoof of horse 5 with tailormade 3D-printed shoes.

The steel shoes, shown in figure 2, that were used in this research project were from Mustad® and had one toe-clip, an 8 mm thick sole and normal size branches. The weight of the shoes was 472.0 ± 85gr.

Figure 2: the lateral and solar view of the left front hoof of horse 5 with steel shoes.

With the start of each shoeing cycle, the hooves were trimmed towards a static hoof balance by experienced farriers at the University of Utrecht. The same farrier trimmed and shod the same pair of horses during the entire project. For the shoeing cycle with the tailormade 3D-printed shoes, the hooves

were scanned with a 3D camera to get a 3D scan of the hoof. This scan was entered in a software program, where the 3D-printed shoe was designed, and adjustments could be made. Three days after the trimming and scanning of the hooves, the tailormade 3D-printed shoes were glued on the hoof with Shufit glue from the brand glue-u ®. The three-day period between the scanning and the application of the tailormade 3D-printed shoes is due to limitations of the printing company. During this three-day period, the hooves were bandaged, and the horses were box rested to prevent the hooves from wearing. For the shoeing cycle with the steel shoes, the protocol of the hoof bandage and box rest was repeated to keep the circumstances the same for both shoeing cycles. The steel shoes were fitted to the hooves and nailed on the hoof with Mustad ® copper nails.

3. Data collection

Kinetics

Force - and pressure plate measurements took place in week 1 (T0) and week 7 (T1) of the shoeing cycle. The kinematic measurements took place prior to the force- and pressure plate measurements which ensured that the horses were well warmed up. The horses were led over the measuring system by one experienced handler, first at walk and later at trot.

The measurement system, illustrated in figure 3, consisted of a composite pressure-force system where the 1-meter-long pressure plate (PP) (Footscan 3D®, RsScan International) was mounted on top of the force plate (FP) (Z4852C, Kistler) embedded in the middle of a 20 m long track, covered by a 5 mm rubber mat. FP and PP data were collected simultaneously and recorded on a notebook computer (HP Compaq Business notebook 6730b®) with dedicated software (Footscan 7® - RsScan International).

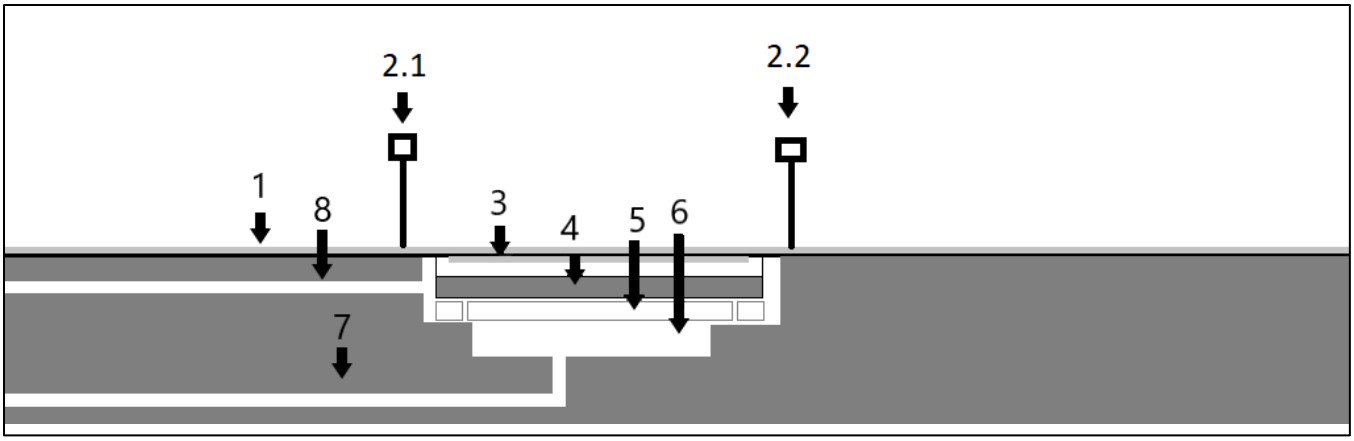

Figure 3: composite pressure - force system. 1: rubber mat, 2: photo-electronic sensors; 2.1 start gate and 2.2 stop gate, 3: pressure plate, 4: force plate, 5: steel construction, 7: drainage, 8: cable.

The FP is calibrated by the Kistler company. They create a calibration file which can be used to calibrate the plate before each measurement session. The PP is sent to and calibrated at the Footscan 3D® company. A CD-ROM with the calibration specifics is created to calibrate the PP at the start of the research project. The composite pressure-force system was calibrated with no weight on or near the plate before measurements took place and got recalibrated in between horses to avoid drift. The FP was triggered by the weight of the horse when the hooves touched the plate and the PP, in turn, was triggered by the FP.

The average velocity over the measuring area was recorded using two pairs of photoelectric-sensors (WE260-S270, Sick) that were placed as two gates, 2 metres apart, perpendicular to the runway centred over the measuring area, connected to an electronic timing box (Timer Interval Meter K3HB-P, Omron). The acceleration was not measured on the track, however, the track was long enough to reach a constant pace over the measuring area and thus long enough to minimise the effect of acceleration and deceleration at the start and end of each trial. The horses were walked and trotted at a pre-set velocity range of 0.9-1.5 m/s at walk and 1.8-3.5 m/s at trot. The pre-set velocity range limits the influence of

speed on the results. A trial was considered valid if the horse moved at a constant pace within the pre-set range while looking forward and fully contacting the plate surface with one forelimb. For walk and trot, five valid measurements were required for each forelimb.

Hoof conformation

The farriers measured the toe angle with a farrier's gauge at two timepoints: before application of the shoes (D0) and after removal of the shoes (DX). In addition, hoof pictures were taken before application of the shoes (D0) and after removal of the shoes (DX) to determine the hoof conformation changes. Pictures were taken from the frontal and lateral view of the left and right forehoof by a Canon Powershot A650IS camera while the horse was standing square. The camera was attached to a mount which was equipped with a level and two pins, as illustrated in figure 4. These pins were later used to calibrate the picture in an application.

Figure 4: the camera construction; level (highlighted with the white circle) and pins (highlighted with the black circle), for the hoof pictures.

Shoe wear characteristics

The steel shoes and tailormade 3D-printed shoes were weighed before applying the shoe to the horse and after removal of the shoe to determine the amount of wear. The steel shoes were weighed without nails. For the tailormade 3D-printed shoes, the glue residue was removed as much as was achievable before weighing them. The distribution of wear was visible with the help of the solar view hoof pictures which were taken weekly. For the 3D-printed shoes, the distribution of wear is visible through the alternating blue and white lines, as seen in figure 5.

Figure 5: the solar view of the left front hoof of horse 4 with tailormade 3D-printed shoes in week 1, week 4 and week 7.

For the steel shoe, however, the distribution of wear is not that easily seen on the solar picture, as seen in figure 6. The wear around the nails gives little insight to the distribution of wear.

Figure 6: the solar view of the left front hoof of horse 4 with steel shoes in week 1, week 4 and week 7.

4. Data analysis

Kinetics

The kinetic parameters were calculated for the left and right forelimb for five valid measurements at walk and trot. In the Footscan 7® software, the landing orientation was determined manually, and the footprints were divided into 4 regions while excluding measurements that were not useable. After exporting the raw data from the FP and PP, the data was further processed using custom-made MATLAB® scripts. For all trials, the kinetic parameters shown in table 2 were calculated.

Table 2: overview of the kinetic variables to be evaluated. Each variable is quantified for at least the right and left front limbs. These variables are measured for the stance phase only. FP: force plate; PP: pressure plate.

Kinetic variable	Units	Measuring tool	Description
Peak vertical force (PVF)	Newton per kilogram (N/Kg)	FP	Highest vertical ground reaction force (GRF), normalised by the horse's body mass
Vertical impulse (VI)	Newton*seconds per kilogram (N.s/kg)	FP	Integral of vertical force over a time period, calculated by time integration of time for curves and normalised by the horse's body mass
Stance duration (StDur)	Seconds (s)	PP	Time period in which the hoof is in contact with the ground
tPVF	Seconds (s)	FP	Time to the peak vertical force
PVF-to-lift-off	Seconds (s)	FP	Time from the peak vertical force to the lift off of the hoof
Time-of-zero at the GRFy	Seconds (s)	FP	Time point on the Fy graph where the deceleration force turns into the propulsive force (corresponds with the midstance)
Landing orientation	Percentage (%)	PP	Initial hoof contact expressed in different regions: heel flat, heel lateral, heel medial, branch flat, branch lateral, branch medial, toe flat, toe lateral and toe medial
Peak pressure distribution	Newton per cubic centimetre (N/cm^2)	PP	Peak pressure under the different hoof areas, calculated by dividing the hoof in four regions with the help of two perpendicular lines (one through the maximal hoof width and one through the central part of the toe and the midway of the heel region)

Table 2: continued.

Kinetic variable	Units	Measuring tool	Description
StDur toe-heel index	Percentage (%)	PP	Dynamic ratio of the contribution between the lateral and medial parts of the hoof, calculated with the help of ASI formulas*
StDur medial-lateral index	Percentage (%)	PP	Dynamic ratio of the contribution between the toe and heel parts of the hoof, calculated with the help of ASI formulas*

* The StDur indexes were calculated by asymmetry indices (ASI) using the following formulas (Sleutjens et al., 2018):

$$StDur\ toe - heel\ index\ = \frac{StDur(toe) - StDur(heel)}{0.5\ *\ \left(StDur\ (toe) + StDur(heel)\right)} * 100$$

$$StDur\ medial - lateral\ index = \frac{StDur(medial) - StDur(lateral)}{0.5 * \ (StDur(medial) + StDur(lateral))}\ *\ 100$$

A positive ASI value indicates higher contribution of the toe zone respectively medial zone to the stance phase whereas, a negative ASI value indicates higher contribution of the heel zone respectively lateral zone to the stance phase.

The ASI data was normalised to the percentage of stance time to compare the data obtained from different measurements.

Hoof conformation

The toe angles that were measured by the farriers were collected in an Excel sheet. The bare hoof pictures from week 0 (T0) and week 7 (T1) were loaded into a custom-made MATLAB® application, the HoofProject application. The software was able to determine lengths and angles through manual selection of landmarks, as illustrated in figure 7.

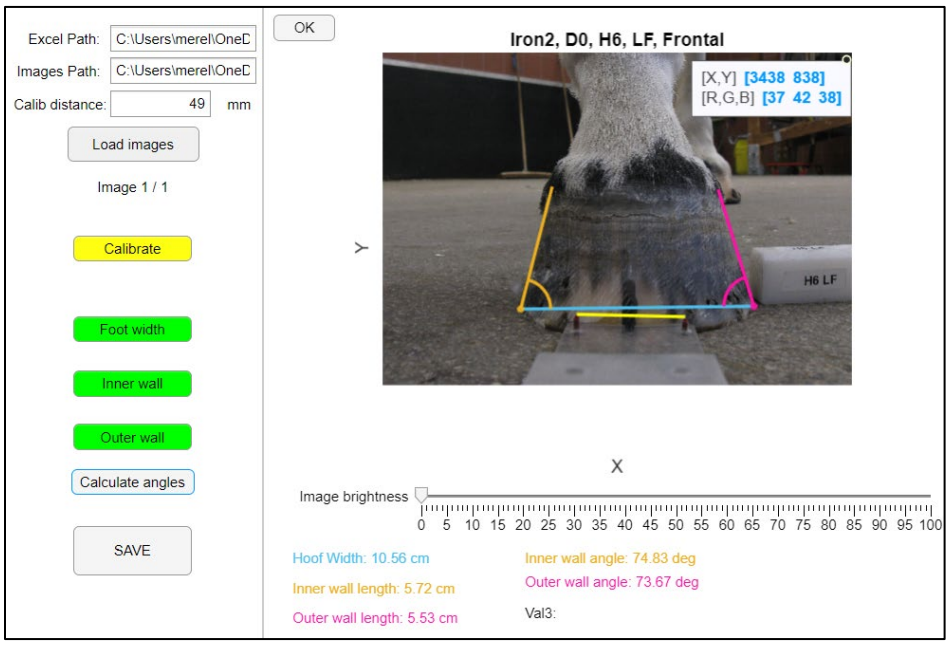

Figure 7: an example of the selected landmarks in the HoofProject application.

The manual selection of the landmarks is time consuming as there are 2 views per hoof. Therefore, a left or right hoof was chosen to process by random selection for each individual horse, as seen in table 3.

Horse	H1	H2	H3	H4	H5	H6
Hoof	Left	Right	Left	Left	Right	Right

Table 3: the random selection of the hoof per horse.

To minimise errors, each picture was processed 10 times, the 5 values that were the furthest from the median were removed which left a “trimmed” data set. The average of the remaining 5 outcomes was used for further analysis. The outcomes that were measured in the frontal and lateral view are shown in table 4 and collected in an Excel sheet.

Frontal view	Lateral View
Hoof width (mm)	Hoof length (mm)
Inner wall length (mm)	Toe length (mm)
Outer wall length (mm)	Heel length (mm)
Inner wall angle (degrees)	Toe angle (degrees)
Outer wall angle (degrees)	Heel angle (degrees)

Table 4: the view of the hoof and the outcomes measured with the HoofProject application.

Shoe wear characteristics

To analyse the wear of the shoes, the weight after removal of the shoe was subtracted from the weight before the application of the shoe. The outcome was expressed in grams.

For the distribution of wear, the hoof was divided into four regions: medial heel, lateral heel, medial toe, and lateral toe. These four regions were specified with the help of two perpendicular lines (one through the maximal hoof width and one through the central part of the toe and the midway of the heel region), as seen in figure 8.

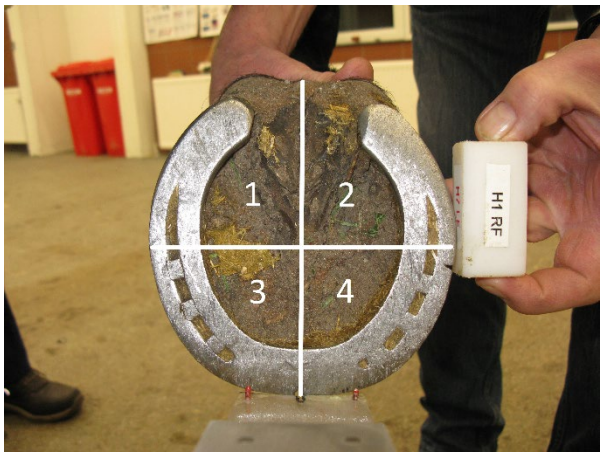

Figure 8: solar view of the right front hoof of horse 1 in week 7 with steel shoes as an example how the 4 hoof regions (numbers) are specified by two perpendicular lines (white lines). 1. medial heel, 2. lateral heel, 3. medial toe, 4. lateral toe.

The solar pictures of week 7 were analysed to determine in which regions the shoe wore. The outcome was expressed with the help of a scale, as seen in table 5.

	Scale for wear distribution of the shoe
Scale number	**Description scale**
I	absence of wear/almost invisible wear
II	slightly worn but no damage to the shoe
III	visibly worn/little damage to the shoe
IV	clearly worn/shoe damaged
V	completely worn/hoof is showing under the shoes

Table 5: scale to express the wear distribution of the shoe.

Two solar pictures of week 7, one of each shoeing cycle, were used to compare the other pictures to, to ensure uniformity in classifying the pictures, as seen in figure 9 and figure 10. In these pictures scale number I up to and including number IV are illustrated for the steel shoeing cycle and the tailormade 3D printed shoeing cycle per hoof region.

Figure 9: solar view of the right front hoof of horse 2 in week 7 with steel shoes. The wear distribution of the shoe in the four regions was classified with the help of the scale for wear of the shoe mentioned above. Medial heel:I , lateral heel: III: , medial toe: II, lateral toe: IV.

Figure 10: solar view of the right front hoof of horse 4 in week 7 with tailormade 3D-printed shoes. The wear distribution of the shoe in the four regions was classified with the help of the scale for wear of the shoe mentioned above. Medial heel: I, lateral heel: III, medial toe: II, lateral toe: IV.

Missing data

Kinetics

Just before the measurements of horse 5 at week 1 (T0) of the tailormade 3D-printed shoeing cycle, the pressure plate had a broken sensor. Another stand-alone pressure plate was used to measure the kinetic parameters obtained from the pressure plate. These values did not correspond with values found with the composite pressure-force system that was used during the rest of this research. To meet the assumption of normal distribution, the outcomes were not included in this research paper. Furthermore, the measurements of horse 5 week 7 (T1) of the tailormade 3D-printed shoeing cycle did not take place as the horse was deemed lame by a vet.

Due to missing data in the first regular iron shoeing cycle, only the data from the second regular iron shoeing cycle is used in analysing. Moreover, only data of the trials in trot were used in this paper as there were too little trials in walk for some horses.

Hoof conformation

For horse 5 and horse 6, no bare pictures after removal of the shoe were available for the steel shoeing cycle. Pictures of the shod hooves were taken instead. To ensure shod pictures did not differ from the bare pictures, a trial was conducted to see if there was any significant difference in outcome between the bare pictures and shod pictures using the Hoofproject application. A Shapiro Wilk's test was used to ensure normal distribution and the data was tested with a paired t-test and a statistical significance set at $p\ value \leq .05$.

The outcomes of the hoof conformation variables showed noticeable differences at T0 between the shoeing conditions. As a result, the two shoeing conditions were not compared to each other. Only the hoof conformation changes over time were tested and compared between the shoeing conditions.

Shoe wear characteristics

Due to the glue residue in the tailormade 3D-printed shoes, it was not possible to get the accurate weights of the tailormade 3D-printed plastic shoes after removal of the shoe. The data is visualised in a boxplot but was not statistically tested.

For horse 1 and horse 2, it was not possible to remove any glue from the tailormade 3D-printed shoes. The outcomes for the wear of the tailormade 3D-printed shoes of horse 1 and horse 2 were not included in the data analysis of the amount of wear of the shoes. These outcomes were thus documented as NA (not available).

5. Statistical analysis

Data were collected and prepared for statistical analysis using custom-made MATLAB® codes and spreadsheet software (Microsoft Excel). The data is presented as estimated mean ± SD, unless stated otherwise. The statistical analysis was performed using the open Software Rstudio. To compare the discrete variables, such as GRF parameters, pressure distribution ratios and hoof conformation parameters in time and between the shoeing conditions a linear mixed effect model was used with a statistical significance set at $p\ value \leq .05$ (unless stated otherwise). The model was constructed with shoeing condition and timepoints as fixed effects and horse and hoof as random effects. The data was checked for normal distribution by plotting QQ plots, density plots and Gaussian plots of the residuals of the linear mixed model described. After the linear mixed effect model, a pairwise comparison was performed.

II. Results

Kinetics

Force plate

Kinetic variables obtained by the FP with their p-value are presented in table 6. When comparing both shoeing conditions, the VI and PVF were significantly higher for the tailormade 3D-printed shoes compared to the steel shoes at both timepoints (table 6). Furthermore, the time-of-zero-GRFy was significantly longer (table 6) at T1 in the tailormade 3D-printed shoes compared to the steel shoes.

Table 6: kinetic variables measured with the FP per shoeing condition (tailormade 3D-printed shoes (Plastic) and steel shoes (Steel)) and timepoint (T0 and T1).

Kinetic variable	**Shoeing condition**	**Timepoint**	**Estimated mean**	**Standard error**	***p value T0-T1***	***p value Steel shoes - Plastic shoes***
StDur (s)	Steel	T0	0.33	0.005		
	Steel	T1	0.32*	0.005	.048	
	Plastic	T0	0.33	0.005		.824
	Plastic	T1	0.33†	0.005	.977	.001
VI (N.s/kg)	Steel	T0	1354.4	51.0		
	Steel	T1	1224.0	51.9	.077	
	Plastic	T0	1533.4•	51.2		.005
	Plastic	T1	1518.7†	51.4	.993	<.001
PVF (N/kg)	Steel	T0	6.6	0.3		
	Steel	T1	6.2	0.3	.424	
	Plastic	T0	7.6•	0.3		.001
	Plastic	T1	7.5†	0.3	.999	<.001

Table 6: continued.

Kinetic variable	**Shoeing condition**	**Timepoint**	**Estimated mean**	**Standard error**	***p value T0-T1***	***p value Steel shoes - Plastic shoes***
tPVF (s)	Steel	T0	0.15	0.003		
	Steel	T1	0.14	0.003	.073	
	Plastic	T0	0.15	0.003		.060
	Plastic	T1	0.15†	0.003	.435	.004
tPVF to lift off (s)	Steel	T0	0.18	0.003		
	Steel	T1	0.19	0.003	.198	
	Plastic	T0	0.18	0.003		.815
	Plastic	T1	0.18†	0.003	.183	.011
Time of zero at GRFy (s)	Steel	T0	0.05	0.002		
	Steel	T1	0.05	0.002	.924	
	Plastic	T0	0.05	0.002		.993
	Plastic	T1	0.06*†	0.002	.005	.018
Speed trial (m/s)	Steel	T0	2.4	0.04		
	Steel	T1	2.5	0.04	.613	
	Plastic	T0	2.3	0.04		.251
	Plastic	T1	2.3†	0.04	.944	.005

** Significant difference (p value < .05) T1 compared to T0 in a shoeing cycle. • Significant difference (p value < .05) tailormade 3D-printed shoes compared to steel shoes at T0. † Significant difference (p value < .05) tailormade 3D-printed shoes compared to steel shoes at T1.*

Pressure plate

The preferred landing in both the shoeing conditions and timepoints was the lateral heel, as shown in figure 11.

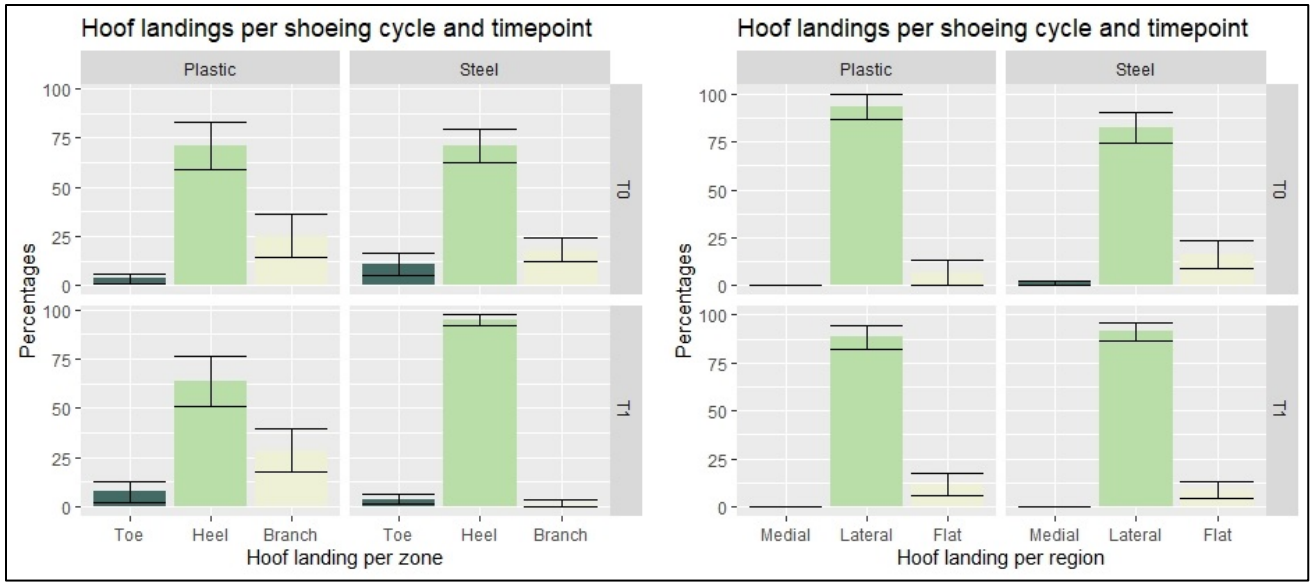

Figure 11: barplots of the hoof landings per zone (left) and region (right) in percentages per shoeing condition (tailormade 3D-printed shoes (Plastic) and steel shoes (Steel)) and timepoint (T0 and T1).

The peak pressures extracted from the PP data and their corresponding p-values are presented in table 7. At T0, the peak pressure in all hoof regions (lateral heel, medial heel, lateral toe and medial toe) was significantly higher in the tailormade 3D-printed shoes compared to the steel shoes (table 7)

Table 7: peak pressure within each hoof region measured with the PP per shoeing condition (tailormade 3D-printed shoes (Plastic) and steel shoes (Steel) and timepoint (T0 and T1).

Kinetic variable	**Shoeing condition**	**Timepoint**	**Estimated mean**	**Standard error**	***p value T0-T1***	***p value Steel shoes - Plastic shoes***
Lateral Heel (N/cm^2)	Steel	T0	21.5	1.7		
	Steel	T1	25.1*	1.7	<.001	
	Plastic	T0	36.8•	1.7		<.001
	Plastic	T1	36.5†	1.7	.992	<.001

Table 7: continued.

Kinetic variable	**Shoeing condition**	**Timepoint**	**Estimated mean**	**Standard error**	***p value T0-T1***	***p value Steel shoes - Plastic shoes***
Medial Heel (N/cm^2)	Steel	T0	32.4	2.0		
	Steel	T1	42.2*	2.0	<.001	
	Plastic	T0	43.9•	2.1		<.001
	Plastic	T1	41.1	2.0	.249	.865
Heel total (N/cm^2)	Steel	T0	54.0	3.1		
	Steel	T1	67.2*	3.1	<.001	
	Plastic	T0	80.6•	3.2		<.001
	Plastic	T1	77.5*†	3.1	.422	<.001
Lateral toe (N/cm^2)	Steel	T0	32.8	1.0		
	Steel	T1	36.7*	1.0	<.001	
	Plastic	T0	37.5•	1.0		<.001
	Plastic	T1	33.9*	1.0	<.001	<.001
Medial toe (N/cm^2)	Steel	T0	42.8	0.9		
	Steel	T1	44.8*	0.9	.032	
	Plastic	T0	45.1•	0.9		.020
	Plastic	T1	38.2*†	0.9	<.001	<.001
Toe total (N/cm^2)	Steel	T0	75.6	1.6		
	Steel	T1	81.5*	1.6	<.001	
	Plastic	T0	82.6•	1.6		<.001
	Plastic	T1	72.1*†	1.6	<.001	<.001

** Significant difference (p value < .05) T1 compared to T0 in a shoeing cycle. • Significant difference (p value < .05) tailormade 3D-printed shoes compared to steel shoes at T0. † Significant difference (p value < .05) tailormade 3D-printed shoes compared to steel shoes at T1.*

The peak pressure distribution in percentages was calculated through the absolute peak pressure values. The peak pressure in the hoof regions in the tailormade 3D-printed shoes appears to be more homogenous distributed compared to the steel shoes at both timepoints, as seen in figure 12.

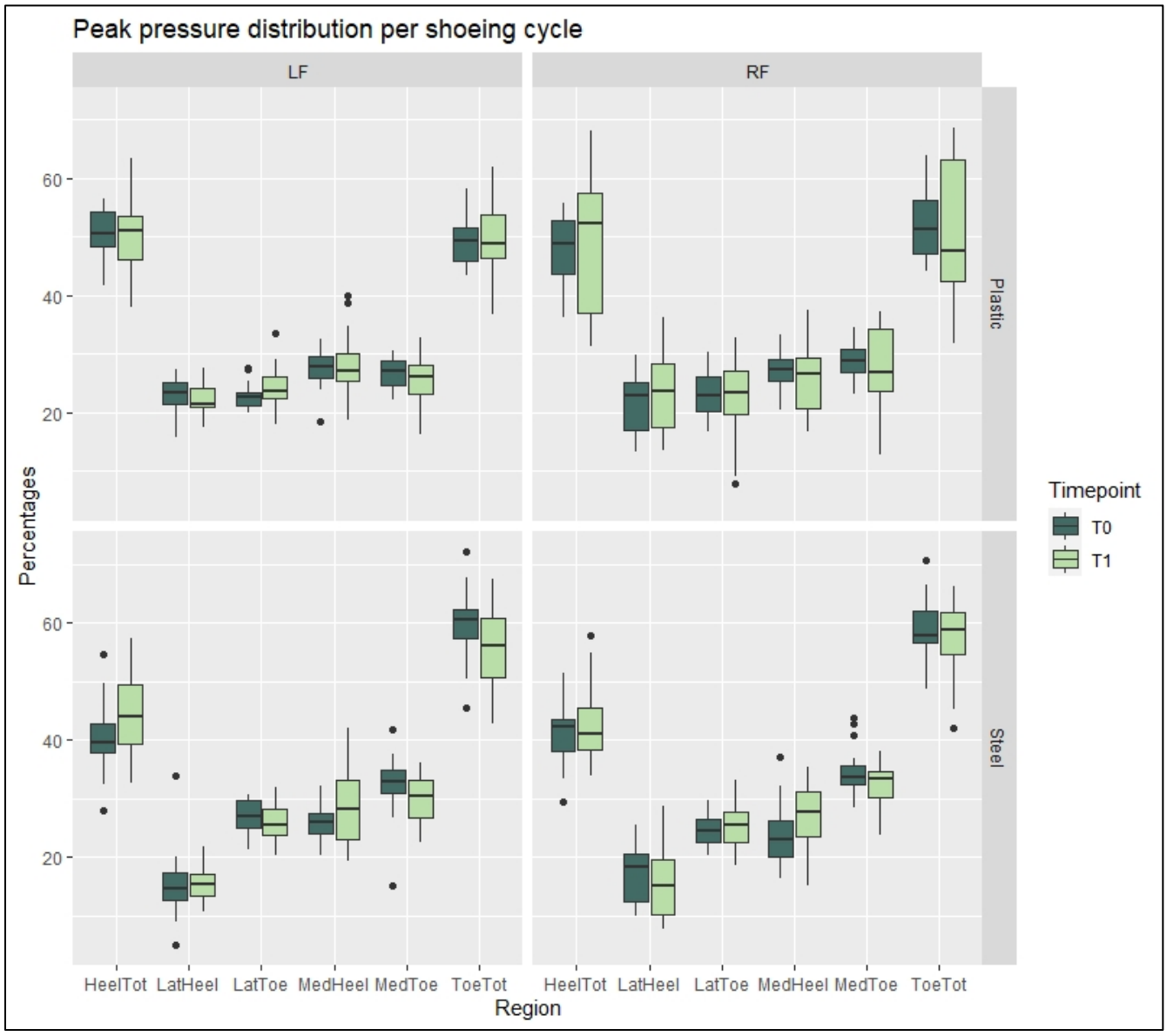

Figure 12: boxplot of the peak pressure per region in percentages per shoeing condition (tailormade 3D-printed shoes (Plastic) and steel shoes (Steel)), hoof (left hoof (LF) and right hoof (RF) and timepoint (T0 and T1). Heeltot = total heel pressure, LatHeel = lateral heel pressure, LatToe = lateral toe pressure, MedHeel = medial heel pressure, MedToe = medial toe pressure, ToeTot = total toe pressure.

The StDur toe – heel index and StDur medial – lateral index and their corresponding p-values can be found in table 8. At T1, the StDur toe – heel index was significantly higher in the tailormade 3D-printed shoes compared to the steel shoes while the StDur medial – lateral index was significantly lower in the tailormade 3D-printed shoes compared to the steel shoes (table 8).

Kinetic variable	**Shoeing condition**	**Timepoint**	**Estimated mean**	**Standard error**	***p value T0-T1***	***p value Steel shoes - Plastic shoes***
StDur toe – heel index	Steel	T0	14.5	0.8		
	Steel	T1	13.7	0.8	.610	
	Plastic	T0	15.4	0.9		.420
	Plastic	T1	15.2†	0.8	.988	.049
StDur medial – lateral index	Steel	T0	9.3	1.4		
	Steel	T1	12.4*	1.4	.007	
	Plastic	T0	9.4	1.4		.999
	Plastic	T1	3.7*†	1.4	<.001	<.001

Table 8: StDur toe – heel index and StDur medial – lateral index measured with the PP per shoeing condition (tailormade 3D-printed shoes (Plastic) and steel shoes (Steel)) and timepoint (T0 and T1).
** Significant difference (p value < .05) T1 compared to T0 in a shoeing cycle. † Significant difference (p value < .05) tailormade 3D-printed shoes compared to steel shoes at T1.*

Hoof conformation

Toe angle – farriers

The toe angles measured by the farriers can be found in the appendix table 12 and table 13. The toe angle change in the shoeing cycles between timepoints and their corresponding p-values are presented in table 9. In both shoeing conditions, the toe angle decreased significantly between the timepoints (table 9).

Shoeing condition	Estimated mean	Standard error	*p value T0-T1*
Steel	-1.38º	0.63	.035*
Plastic	-1.86º	0.64	.006*

*Table 9: toe angle changes (decrease (-) or increase (+)), measured by the farriers, per shoeing condition (tailormade 3D-printed shoes (Plastic) and steel shoes (Steel)). * Significantly different between T0 and T1.*

The tailormade 3D-printed plastic shoeing cycle had a slightly greater decrease of the toe angle in time compared to the steel shoeing cycle (figure 13).

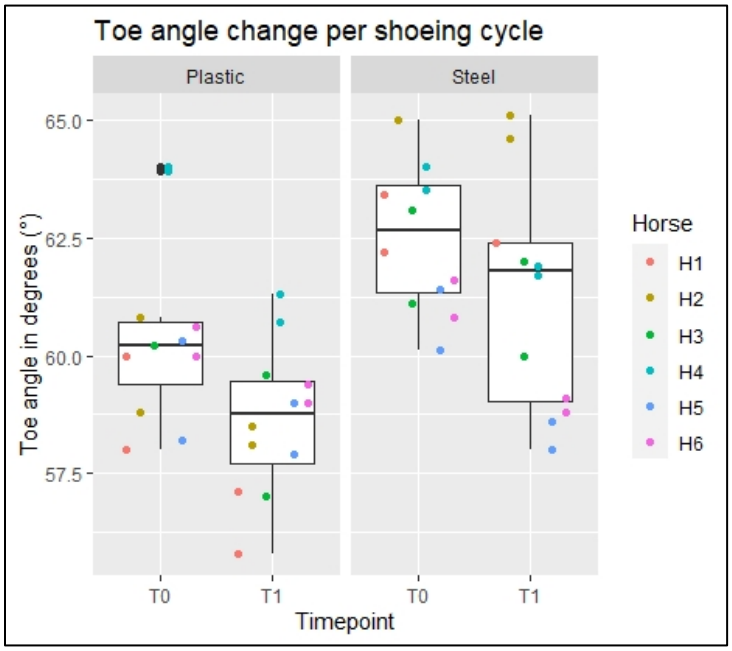

Figure 13: boxplot of the toe angle, measured by the farriers, per shoeing condition (tailormade 3D-printed shoes (Plastic) and steel shoes (Steel)) and timepoint (T0 and T1).

Hoof conformation - HoofProject

As mentioned before, there were no bare pictures available for horse 5 and horse 6 after removal of the shoe for the steel shoeing cycle. In comparing unshod hooves with shod hooves, only the toe length altered significantly (*p value* = .049) between the unshod and shod condition with respectively 6.8 cm

and 6.4 cm. All other hoof conformation variables had no significant difference between the unshod and shod condition. The pictures of the shod hooves of horse 5 and horse 6 were thus included in the data set to increase the amount of data. Table 14 up to and including table 19 in the appendix contain outcomes of the hoof conformation per individual horse. The changes in hoof conformation variables in both shoeing cycles and their p-values can be found in table 10.

Hoof conformation variable	**Shoeing condition**	**Estimated mean**	**Standard error**	***p value T0-T1***
Hoof width	Steel	+0.17	0.06	.009*
	Plastic	+0.21	0.06	.002*
Inner wall length	Steel	+0.20	0.14	.170
	Plastic	+0.36	0.14	.023*
Outer wall length	Steel	+0.30	0.08	.004*
	Plastic	+0.35	0.08	.001*
Inner wall angle	Steel	-0.59	0.75	.443
	Plastic	-0.87	0.75	.266
Outer wall angle	Steel	-0.23	0.72	.751
	Plastic	-0.08	0.72	.915
Hoof length	Steel	+0.50	0.16	.008*
	Plastic	+0.02	0.16	.876
Heel length	Steel	+0.28	0.16	.101
	Plastic	+0.71	0.16	.001*
Toe length	Steel	+0.34	0.13	.016*
	Plastic	+0.75	0.13	.001*
Heel angle	Steel	+1.76	1.67	.308
	Plastic	-0.54	1.67	.753
Toe angle	Steel	-2.02	0.71	.0119*
	Plastic	-1.95	0.71	.0144*

*Table 10: hoof conformation changes (decrease (-) or increase (+)), determined with the help of the HoofProject application, per shoeing condition (tailormade 3D-printed shoes (Plastic) and steel shoes (Steel)). * Significantly different between T0 and T1.*

Shoe wear characteristics

Amount of wear

The weight of the horseshoes per shoeing cycle can be found in the appendix, table 20. The two highest values in the steel shoeing cycle in figure 14 correspond to horse 2 who had larger hooves compared to the rest of the horses.

The weight of the steel shoes is substantially more than the weight of the tailormade 3D-printed shoes. The plots, in figure 14, show a marginally higher wear in the tailormade 3D-printed shoes compared to the steel shoes.

Figure 14: boxplot and spaghetti plot of the weight of the horseshoes per shoeing condition (tailormade 3D-printed shoes (Plastic) and steel shoes (Steel)) and timepoint (T0 and T1).

Wear distribution

The wear distribution of the individual horse per shoeing cycle can be found in the appendix, table 21.

The wear distribution in the tailormade 3D-printed shoes appeared to be more evenly distributed

between the four regions compared to the steel shoe, illustrated in figure 15. The tailormade 3D-printed shoes were overall more worn compared to the steel shoe.

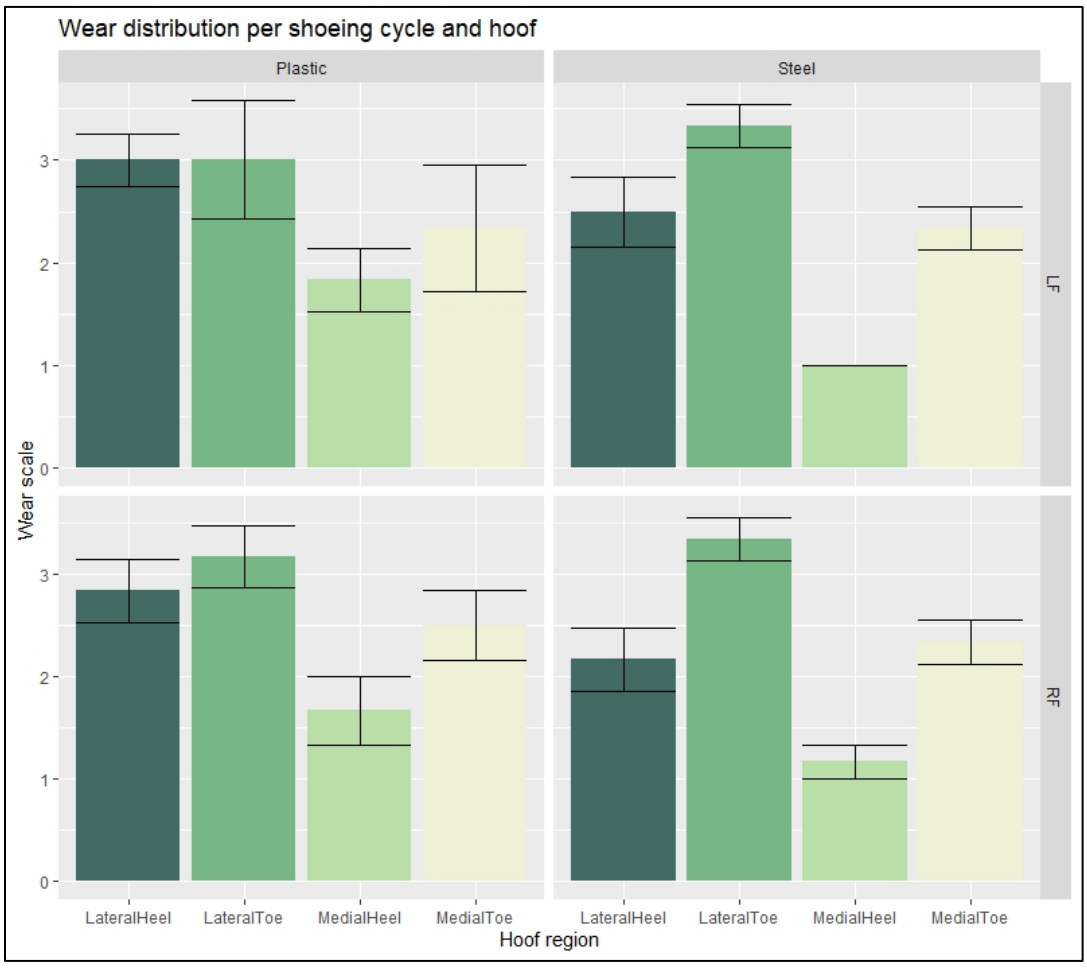

Figure 15: barplot of the wear distribution per region for both shoeing conditions condition (tailormade 3D-printed shoes (Plastic) and steel shoes (Steel)) and hooves (left hoof (LF) and right hoof (RF)). Wearscale: 0 – 5.

III. Final conclusions and future perspective

1. Discussion

This is the first study to investigate the effects of the tailormade 3D-printed horseshoes on kinetic parameters. The results do not support the hypothesis that the tailormade 3D-printed shoes had no influence on the ground reaction forces. The PVF varies with the body mass of the horse, the speed and how much force the horse exerts on its limb (Clayton & Hobbs, 2019). The higher PVF and VI at T0 and T1 found in horses wearing the tailormade 3D-printed shoes could be the result of an increased amount of force exerted by the horse on its limb which could suggest that the horses were more comfortable. The study of Back et al. (2009) in which was shown that lame horses treated with non-steroidal anti-inflammatory drugs (NSAIDs) had a higher PVF and improved lameness scores supports this suggestion (Back et al., 2009). This theory was also suggested in research conducted by Sleutjens et al. (2018), in which normal and obese ponies were shod with mouldable, thermoplastic, glue-on-frog-supportive shoes: higher PVF and VI were measured in the ponies wearing the shoes (Sleutjens et al., 2018). The tailormade 3D-printed shoes were compared to steel shoes which differ in shape and material from each other. This made it impossible to attribute the effects of the tailormade 3D-printed shoes on the GRF to the shape or the material of the shoes as both differed between the shoeing conditions.

The increased time-of-zero-GRFy at T1 in the tailormade 3D-printed shoes and thus less abrupt braking of the distal limb could lead to less ‘jarring’ of the limb as shortened slip times are assumed to be associated with higher forces in the musculoskeletal system at impact (Back et al., 1995; Johnston et al., 1995; Willemen, 1997).

The tPVF, tPVF-to-lift-off and PVF influence the loading- and unloading rate of the limb which were not calculated in this research paper. It would be interesting to evaluate the loading- and unloading rate

in both shoeing conditions as it is known that an increased loading rate can cause pathologies like osteoarthritic change due to higher stress on the limbs (Radin et al., 1985).

In this study, the preferred way of landing in both shoeing conditions and timepoints was lateral heel. This is in accordance with findings in previous studies (Eliashar et al., 2002; van Heel et al., 2004). As hypothesised, there were significant differences in pressure distribution between the shoeing conditions at the timepoints (T0 and T1). The higher peak pressure in all hoof regions in the tailormade 3D-printed shoes at T0 could be explained by the higher PVF in the tailormade 3D-printed shoes. With a similar PVF in both shoeing conditions, it would be expected that the peak pressure is smaller in the tailormade 3D-printed shoes as the contact area with the surface in these shoes is larger compared to the steel shoes. This effect was found in previous research where eggbar shoes were compared to plain shoes (Rogers & Back, 2007).

The increase in peak pressure in the steel shoes at T1 without an increase in PVF suggests a decrease in contact area. This could be explained by the wear distribution of the steel shoes. There was an uneven wear of the steel shoes which could lead to a decreased contact area on hard surfaces as some regions of the hoof wore less compared to other regions. The decrease in peak pressure in the tailormade 3D-printed shoes at T1 could be explained by the decrease in PVF.

The homogeneous peak pressure distribution in the tailormade 3D-printed shoes at both timepoints suggests that the hoof regions received an equal peak pressure during the stance phase. This could be the result of a better distribution of the loads under the shoe area, and thus under the hoof in the tailormade 3D-printed shoes.

At T1, the toe region contributed relatively more to the stance phase compared to the heel region in the tailormade 3D-printed shoes compared to the steel shoes. This could potentially be contraindicative in

horses with laminitis as orthopaedic aid focuses on minimising the load on damaged lamellae in the toe region (Parks et al., 1999). Modifications to the tailormade 3D-printed shoes like incorporating a heel wedge could be beneficial when applying the tailormade 3D-printed shoes for a longer period of time in horses with laminitis. On the other hand, the peak pressure is evenly distributed between the toe- and heel region in the tailormade 3D-printed shoes whereas the steel shoes had higher peak pressures in the toe region compared to the heel region which suggest that the tailormade 3D-printed shoes could be a better option in horses with laminitis compared to steel shoes. The StDur Medial – Lateral index at T1 indicates more balance between the medial - and lateral contribution of the hooves with the tailormade 3D-printed shoes compared to the steel shoes. Imbalance in the medial - and lateral loading of the hoof could attribute to quarter cracks or pedal osteitis (Parks, 2011).

This study was the first to use the in-house HoofProject application to determine hoof conformation variables. The standard deviation approached or exceeded the hoof conformation changes in both shoeing conditions for the inner wall angle, outer wall angle and heel angle, and in the tailormade 3D-printed shoes for the hoof length. This indicates that the precision of selecting the landmarks was insufficient to measure these outcomes. Interpreting the results from these variables should be done with caution. Further research is being conducted to evaluate the accuracy and precision of the application to interpret this high standard deviation compared to the amount of change in hoof conformation.

In comparing hoof conformation variables between unshod hooves and shod hooves, to include the pictures of the shod hooves of horse 5 and horse 6 for their steel shoeing cycle, only the toe length altered significantly. This is most likely due to the shoe clip that covers the toe which could decrease the precision of selecting the toe landmark in the application.

Most of the hoof conformation variables determined with the HoofProject application showed a noticeable difference in outcome at T0 between both shoeing conditions. A study by Kummer et al. (2009) showed that there were significant differences in hoof conformation parameters between two consecutive trimming procedures by the same farrier which could explain the difference in hoof conformation variables measured at T0 (Kummer et al., 2009). Moreover, this study was not blinded. The farriers had knowledge over the shoeing condition before trimming the hooves which could have influenced the way of trimming. Steel shoes with toe clips are seated to the hoof wall by trimming and rasping the hoof wall at the toe which could also influence the outcome of the hoof conformation variables between the shoeing conditions.

As the hoof grows, all the hoof conformation lengths and – widths are expected to increase for both shoeing conditions. In both shoeing conditions the hoof width increased substantially, which implies that the inner- and outer wall lengths increased. The outer wall length increased significantly for both shoeing conditions whereas the inner wall length only increased significantly for the tailormade 3D-printed shoes. This could imply that, in the steel shoes, either the hoof grows more laterally compared to medially or the hoof wears more medially compared to laterally. In the steel shoes, the StDur Medial – Lateral index remained high during the shoeing cycle indicating more contribution of the medial region of the hoof to the stance phase. This could result in more wear on the medial side of the hoof, as there is possibly more friction of the hoof with the steel shoe in this region.

The toe length increased significantly in both shoeing conditions while the heel length only increased significantly for the tailormade 3D-printed shoes. In shod horses, the heels wear more than the toes due to the friction between the shoe and the expanding heel during the stance phase (Eliashar, 2007). The steel shoes are not nailed to the hoof at the heel region which allow the heels to slightly expand during

the stance phase whereas the tailormade 3D-printed shoes are glued at the heel region as well and thus limit the friction.

The inner wall length, outer wall length, toe length and heel length increased significantly in the tailormade 3D-printed shoeing cycle while the steel shoeing cycle only had a significant increase for the outer wall and toe lengths. Overall, the hoof conformation variables indicate that the tailormade 3D-printed shoes had a more balanced growth (and/or wear) of the hoof compared to the steel shoes.

The hoof length only significantly increased for the steel shoe and did not change considerably for the tailormade 3D-printed shoes. Horse 3 and horse 4 even had a decrease in hoof length between T0 and T1 in the tailormade 3D-printed shoes which is most likely due to the lack of precision in selecting the landmarks in the HoofProject application.

The toe angle, determined with the help of the HoofProject application, decreased significantly in both shoeing conditions. The decrease in toe angle is suggested to be caused by an increase in dorsal length (toe length) of the hoof (van Heel et al., 2005). This decrease was approximately the same in both shoeing cycles while the toe angle decrease in the farrier's measurements was higher in the tailormade 3D-printed shoes. The measurement methods differed which could explain the difference found in toe angles as the trimming preparations for the seating of the toe clip of the steel shoes could potentially influence the measurement of the toe angle with the farrier's gauge more compared to the Hoofproject application.

When looking at the weight of the horseshoes before application, it becomes apparent that horse 2 had substantially heavier steel shoes compared to the shoes of the other horses. Horse 2 was a heavier horse and had larger hooves compared to the other horses. An increased weight on the limb leads to a more animated trot (Willemen et al., 1997). The weight of the tailormade 3D-printed shoes in horse 2,

however, is similar to the shoes of the other horses. This could potentially overcome the kinetic - and kinematic effects of added weight to the distal limb in horses who have bigger hooves and need shoes. Both the steel shoes and the tailormade 3D-printed plastic shoes lost weight between T0 and T1 due to friction between the shoes and the surface. The tailormade 3D-printed shoes wore more homogenous compared to the steel shoes between the four hoof regions while looking at the wear distribution for both shoeing conditions. In the kinetic measurements, the peak pressure was more evenly distributed in the tailormade 3D-printed shoes which could have resulted in the homogenous wear of the tailormade 3D-printed shoes.

Lastly, the tailormade 3D-printed shoes tended to be more worn at the end of the shoeing cycle compared to the steel shoes. This was expected as steel is more wear-resistant compared to plastic. In horse 5, the shoe had worn so much that the toe was visible and in contact with the surface. This horse was known with pawing during grooming and tacking. However, the protective functionality of a shoe is lost when there is direct contact between the hoof and the surface (Mischler & Hofmann, 2003).

2. Main limitations

This research had a few limitations. The difference in shape between both shoeing conditions made it impossible to attribute the effects of the tailormade 3D-printed shoes on the kinetic parameters to the shape or the material of the shoe.

Secondly, this research project required manual selection in the data analysis like the region and zone division of the hoof prints, obtained with the pressure plate (Oomen et al., 2012; Oosterlinck et al., 2013, 2014), the landing orientation in the Footscan 7 ® software and the manual selection of the landmarks in the Hoofproject application. Furthermore, the research was not blinded as the farriers had knowledge of

the shoeing cycle before trimming the hooves and the researchers knew which shoes were applied to the horse during the measurements. Both could lead to bias in the research project.

The horses used in this research were deemed rider-sound as they were used by the riding school, but the horses were not vet checked prior to their inclusion in this study. Rider/owner-sound horses are not by definition sound (Müller-Quirin et al., 2020). To avoid dropouts during the research project, it could have been useful to have a locomotion examination by a vet prior to inclusion to the research project. Preferably, the horses should have been handled by the same handler every time. However, due to logistic reasons this was not possible. All handlers were used to handling horses.

The pressure plate is not designed to measure horses but humans. The impact and pressure that a horse exerts could reduce the longevity of the pressure plate (PP). During this research project, the PP could not be used during two measurements due to broken sensors. During the data collection for the Hoofproject application, small handling errors of the mount with camera or placement of the mount with camera could have influenced the pictures taken and thus outcomes. In the data collection for the wear of the tailormade 3D-printed shoes it became apparent that the glue residue made it impossible to provide statistical evidence about the difference in the amount of wear between the two shoeing cycles.

3. Future perspectives

To determine whether the effects on the kinetic parameters were a result of the difference in shape or material, the tailormade 3D-printed shoes could be compared to heartbar steal shoes (to evaluate the effect of the material of the shoe) or to 3D-printed shoes of the same material but with the classic shoe shape (to evaluate the effect of the shape of the shoe). Moreover, to provide more information about the

effect of tailormade 3D-printed shoes on kinetic parameters, the barefoot condition should be compared to the tailormade 3D-printed shoes and the steel shoes.

This research was conducted using healthy horses. As the tailormade 3D-printed shoes could potentially be a great personalised therapeutic solution, research to investigate the effects of the tailormade 3D-printed shoes in horses with musculoskeletal problems is indicated.

The HoofProject application was used as a new method to determine the hoof conformation variables. There is a lack of precision in selecting the landmarks in the HoofProject application. Further investigation in this new method and improvements of the application, like automated hoof shape recognition and computer vision, are indicated as this method could have added value in hoof conformation research.

4. Conclusion

This study was the first to explore the effects of tailormade 3D-printed shoes on kinetic parameters, hoof conformation parameters and wear characteristics compared to steel shoes. The increase in VI and PVF could suggest that the horses are more comfortable in the tailormade 3D-printed shoes. This could be attributed to the frog- and heel support and plastic material of the tailormade 3D-printed shoe. Moreover, the prolonged time of zero GRFy indicates a less abrupt braking of the limb. The peak pressure distribution was more homogeneous in the tailormade 3D-printed shoes compare to the steel shoes. This is in accordance with the wear distribution of the tailormade 3D-printed shoes which was more evenly distributed compared the steel shoes. Lastly, the hoof conformation variables indicate a more balanced hoof growth (and/or wear) with the 3D-printed shoes compared to the steel shoes. The tailormade 3D-printed shoes could be a great solution for horses who need a personalised approach. The results encourage further research to unravel the advantages of tailormade 3D-printed horseshoes.

Reference

Back, W., MacAllister, C. G., van Heel, M. C., Pollmeier, M., & Hanson, P. D. (2009). The use of force plate measurements to titrate the dosage of a new COX-2 inhibitor in lame horses. *Equine Veterinary Journal*, *41*(3), 309–312. https://doi.org/10.2746/042516409X397118/FORMAT/PDF

Back, W., & Pille, F. (2013). The role of the hoof and shoeing. In *Equine Locomotion.* (pp. 147–174).

Back, W., Schamhardt, H., Hartman, W., & Barneveld, A. (1995). Kinematic differences between the distal portions of the forelimbs and hind limbs of horses at the trot. *American Journal of Veterinary Research*, *56*(11), 1522–1528. https://pubmed.ncbi.nlm.nih.gov/8585667/

Back, W., van Schie, M. H. M., & Pol, J. N. (2006). Synthetic shoes attenuate hoof impact in the trotting warmblood horse. *Equine and Comparative Exercise Physiology*, *3*(3), 143–151. https://doi.org/10.1017/ecp200691

Balch, O. K., Butler, D., & Collier, M. A. (1997). Balancing the normal foot: hoof preparation, shoe fit and shoe modification in the performance horse. *Equine Veterinary Education*, *9*(3), 143–154. https://doi.org/10.1111/j.2042-3292.1997.tb01295.x

Barnes, G. R. G., & Pinder, D. N. (1974). In vivo tendon tension and bone strain measurement and correlation. *Journal of Biomechanics*, *7*(1), 35–42. https://doi.org/10.1016/0021-9290(74)90068-2

Barrey, E. (1989). La Parole aux Chercheurs 1. Etude comparative des qualites de confort de differents sols equestres. *La Parole Aux Chercheurs*, *1*(3), 18–25.

Barrey, E. (1990). Investigation of the vertical hoof force distribution in the equine forelimb with an instrumented horseboot. *Equine Veterinary Journal*, *22*(9 S), 35–38. https://doi.org/10.1111/j.2042-3306.1990.tb04731.x

Barrey, E. (1999). Methods, applications and limitations of Gait analysis in horses. *Veterinary Journal*, *157*(1), 7–22. https://doi.org/10.1053/tvjl.1998.0297

Barrey, E. (2013). Gaits and interlimb coordination. In *Equine Locomotion.* (pp. 85–97). https://books.google.nl/books?hl=en&lr=&id=dLKFXgYpdqsC&oi=fnd&pg=PA85&dq=gait+and+interlimb+coordination+barrey&ots=IjIW-f5div&sig=D3KyrZyOu42ZbbVWg1VWb95Su3Y

Barrey, E., Landjerit, B., & Wolter, R. (1990). Shock and vibration during the hoof impact on different track surfaces. *Training*, *1*, 94–96. https://hal.inrae.fr/hal-02779465

Baxter, G. M., Stashak, T. S., & Keegan, K. G. (2020). Examination for Lameness. In *Adams and Stashak's Lameness in Horses* (pp. 67–188). Wiley. https://doi.org/10.1002/9781119276715.ch2

Benoit, P., Barrey, E., Regnault, J. C., & Brochet, J. L. (1993). Comparison of the damping effect of different shoeing by the measurement of hoof acceleration. *Cells Tissues Organs*, *146*(2–3), 109–113. https://doi.org/10.1159/000147430

Bertrone, A. L. (2003). Gait analysis for the quantification of lameness. In R. M.W. & S. J. Dyson (Eds.), *Diagnosis and Management of Lameness in the Horse* (pp. 222–225).

Björck, G. (1958). *Studies on the draught force of horses. Development of a method using strain gauges for measuring forces between hoof and ground.* https://www.worldcat.org/title/studies-on-the-draught-force-of-horses-development-of-a-method-using-strain-gauges-for-measuring-forces-between-hoof-and-ground/oclc/5188730

Brunsting, J., Dumoulin, M., Oosterlinck, M., Haspeslagh, M., Lefère, L., & Pille, F. (2019). Can the hoof be shod without limiting the heel movement? A comparative study between barefoot, shoeing with conventional shoes and a split-toe shoe. *Veterinary Journal*, *246*, 7–11. https://doi.org/10.1016/j.tvjl.2019.01.012

Clayton, H. M. (1989). Terminology for the description of equine jumping kinematics. *Journal of Equine Veterinary Science*, *9*(6), 341–348. https://doi.org/10.1016/S0737-0806(89)80073-5

Clayton, H. M. (1990). The effect of an acute hoof wall angulation on the stride kinematics of trotting

horses. *Equine Veterinary Journal*, *22*(9 S), 86–90. https://doi.org/10.1111/j.2042-3306.1990.tb04742.x

Clayton, H. M. (2016). Horse species symposium: Biomechanics of the exercising horse. *Journal of Animal Science*, *94*(10), 4076–4086. https://doi.org/10.2527/jas.2015-9990

Clayton, H. M., & Hobbs, S. J. (2017). The role of biomechanical analysis of horse and rider in equitation science. *Applied Animal Behaviour Science*, *190*, 123–132. https://doi.org/10.1016/j.applanim.2017.02.011

Clayton, H. M., & Hobbs, S. J. (2019). Ground Reaction Forces: The Sine Qua Non of Legged Locomotion. In *Journal of Equine Veterinary Science* (Vol. 76, pp. 25–35). W.B. Saunders. https://doi.org/10.1016/j.jevs.2019.02.022

Crevier-denoix, N., Roosen, C., Dardillat, C., Pourcelot, P., Jerbi, H., Sanaa, M., & Denoix, J.-M. (2001). Effects of heel and toe elevation upon the digital joint angles in the standing horse. *Equine Veterinary Journal*, *33*(S33), 74–78. https://doi.org/10.1111/j.2042-3306.2001.tb05364.x

Drevemo, S., Dalin, G., Fredericson, I., & Hjerten, G. (1980). Equine locomotion; 1. The analysis of linear and temporal stride characteristics of trotting standardbreds. *Equine Veterinary Journal*, *12*(2), 60–65. https://doi.org/10.1111/J.2042-3306.1980.TB02310.X

Eliashar, E. (2007). An evidence-based assessment of the biomechanical effects of the common shoeing and farriery techniques. *The Veterinary Clinics of North America. Equine Practice*, *23*(2), 425–442. https://doi.org/10.1016/J.CVEQ.2007.03.010

Eliashar, E., McGuigan, M. P., Rogers, K. A., & Wilson, A. M. (2002). A comparison of three horseshoeing styles on the kinetics of breakover in sound horses. *Equine Veterinary Journal*, *34*(2), 184–190. https://doi.org/10.2746/042516402776767303

Frederick, F. H. J., & Henderson, J. M. (1970). Impact force measurement using preloaded transducers.

American Journal of Veterinary Research, *31*, 2279–2283. https://www-cabdirect-org.proxy.library.uu.nl/cabdirect/abstract/19712205113

Hagen, J., Hüppler, M., Geiger, S. M., Mäder, D., & Häfner, F. S. (2017). Modifying the Height of Horseshoes: Effects of Wedge Shoes, Studs, and Rocker Shoes on the Phalangeal Alignment, Pressure Distribution, and Hoof-Ground Contact During Motion. *Journal of Equine Veterinary Science*, *53*, 8–18. https://doi.org/10.1016/J.JEVS.2017.01.014

Hoffmann, K. L., Wood, A. K. W., Griffiths, K. A., Evans, D. L., Gill, R. W., & Kirby, A. C. (2001). Doppler sonographic measurements of arterial blood flow and their repeatability in the equine foot during weight bearing and non-weight bearing. *Research in Veterinary Science*, *70*(3), 199–204. https://doi.org/10.1053/rvsc.2001.0461

Jeffcott, L. B., Dalin, G., Drevemo, S., Fredricson, I., Björne, K., & Bergquist, A. (1982). Effect of induced back pain on gait and performance of trotting horses. *Equine Veterinary Journal*, *14*(2), 129–133. https://doi.org/10.1111/j.2042-3306.1982.tb02366.x

Johnston, C., Roepstorff, L., Drevemo, S., & Ronéus, N. (1995). Kinematics of the distal forelimb during the stance phase in the fast trotting Standardbred. *Equine Veterinary Journal*, *27*(18 S), 170–174. https://doi.org/10.1111/J.2042-3306.1995.TB04913.X

Kainer, R. A. (1989). Clinical anatomy of the equine foot. *The Veterinary Clinics of North America. Equine Practice*, *5*(1), 1–27. https://doi.org/10.1016/S0749-0739(17)30601-6

Kummer, M., Gygax, D., Lischer, C., & Auer, J. (2009). Comparison of the trimming procedure of six different farriers by quantitative evaluation of hoof radiographs. *Veterinary Journal (London, England : 1997)*, *179*(3), 401–406. https://doi.org/10.1016/J.TVJL.2007.10.029

Leach, D. H. (1993). Recommended terminology for researchers in locomotion and biomechanics of quadrupedal animals. *Cells Tissues Organs*, *146*(2–3), 130–136. https://doi.org/10.1159/000147434

Leach, D. H., & Crawford, W. H. (1983). Guidelines for the future of equine locomotion research. *Equine Veterinary Journal*, *15*(2), 103–110. https://doi.org/10.1111/j.2042-3306.1983.tb01728.x

Leach, D. H., Ormrod, K., & Clayton, H. M. (1984). Standardised terminology for the description and analysis of equine locomotion. *Equine Veterinary Journal*, *16*(6), 522–528. https://doi.org/10.1111/j.2042-3306.1984.tb02007.x

McMahon, T. A., & Greene, P. R. (1979). The influence of track compliance on running. *Journal of Biomechanics*, *12*(12), 893–904. https://doi.org/10.1016/0021-9290(79)90057-5

Mischler, S., & Hofmann, M. (2003). Wear of polymer horseshoes: a field investigation. *Wear*, *255*(7–12), 1300–1305. https://doi.org/10.1016/S0043-1648(03)00166-2

Moyer, W., & Anderson, J. P. (1975). Lamenesses caused by improper shoeing. *Americal Veterinary Medical Association*, *166*(1), 47–52. https://pubmed.ncbi.nlm.nih.gov/1110198/

Müller-Quirin, J., Dittmann, M. T., Roepstorff, C., Arpagaus, S., Latif, S., & Weishaupt, M. (2020). *Riding soundnessd comparison of subjective with objective lameness assessments of owner-sound horses at trot on a treadmill*. https://doi.org/10.1016/j.jevs.2020.103314

Nigg, B. M. (1983). External force measurements with sport shoes and playing surfaces. In *Biomechanical Aspects of Sport Shoes and Playing Surfaces* (p. 11).

Oomen, A. M., Oosterlinck, M., Pille, F., Sonneveld, D. C., Gasthuys, F., & Back, W. (2012). *Use of a pressure plate to analyse the toe-heel load redistribution underneath a normal shoe and a shoe with a wide toe in sound warmblood horses at the walk and trot*. 1026–1031. https://doi.org/10.1016/j.rvsc.2012.01.010

Oosterlinck, M., Dumoulin, M., Van De Water, E., & Pille, F. (2017). Biomechanische aspecten met betrekking tot hoefbeslag bij paarden. *Vlaams Diergeneeskundig Tijdschrift*, *86*(4), 256–265. https://doi.org/10.21825/vdt.v86i4.16187

Oosterlinck, M., Hardeman, L. C., van der Meij, B. R., Veraa, S., van der Kolk, J. H., Wijnberg, I. D., Pille, F., & Back, W. (2013). Pressure plate analysis of toe-heel and medio-lateral hoof balance at the walk and trot in sound sport horses. *Veterinary Journal*, *198*(SUPPL1). https://doi.org/10.1016/j.tvjl.2013.09.026

Oosterlinck, M., Pille, F., Dumoulin, M., & Gasthuys, F. (2007). Moderne technieken voor kreupelheidsonderzoek bij het paard: beter dan de klinische blik? *Vlaams Diergeneeskundig Tijdschrift*, 91–102. https://biblio.ugent.be/publication/366862

Oosterlinck, M., Pille, F., Huppes, T., Gasthuys, F., & Back, W. (2010). Comparison of pressure plate and force plate gait kinetics in sound Warmbloods at walk and trot. *Veterinary Journal*, *186*(3), 347–351. https://doi.org/10.1016/j.tvjl.2009.08.024

Oosterlinck, M., Pille, F., Sonneveld, D. C., Oomen, A. M., Gasthuys, F., & Back, W. (2012). Contribution of dynamic calibration to the measurement accuracy of a pressure plate system throughout the stance phase in sound horses. *Veterinary Journal*, *193*(2), 471–474. https://doi.org/10.1016/j.tvjl.2012.01.029

Oosterlinck, M., Royaux, E., Back, W., & Pille, F. (2014). A preliminary study on pressure-plate evaluation of forelimb toe-heel and mediolateral hoof balance on a hard vs. a soft surface in sound ponies at the walk and trot. *Equine Veterinary Journal*, *46*(6), 751–755. https://doi.org/10.1111/EVJ.12210

Pardoe, C. H., Mcguican, M. P., Rogers, K. M., Rowe, L. L., & Wilson, A. M. (2001). The effect of shoe material on the kinetics and kinematics of foot slip at impact on concrete. *Equine Veterinary Journal*, *33*(S33), 70–73. https://doi.org/10.1111/j.2042-3306.2001.tb05363.x

Parks, A. H. (2011). The foot and shoeing. In *Diagnosis and Management of Lameness in the Horse* (pp. 282–309).

Parks, Balch, & Collier. (1999). Treatment of acute laminitis supportive therapy. *North Am Equine Pract*, *15*, 363–374.

Pietra, M., Guglielmini, C., Nardi, S., Gandini, G., & Cipone, M. (2004). Influence of weight bearing and hoof position on Doppler evaluation of lateral palmar digital arteries in healthy horses. *American Journal of Veterinary Research*, *65*(9), 1211–1215. https://doi.org/10.2460/ajvr.2004.65.1211

Pratt, G. W., & O'Connor, J. T. (1976). Force plate studies of equine biomechanics. *American Journal of Veterinary Research*, *37*(11), 1251–1255. https://europepmc.org/article/med/984554

Radin, E., Martin, R., Burr, D., Caterson, B., Boyd, R., & Goodwin, C. (1985). Mechanical factors influencing cartilage damage. In: Osteoarthritis: Current Clinical and Fundamental Problems. In *Osteoarthritis: Current Clinical and Fundamental Problems* (pp. 90–99).

Ratzlaff, M. H., Hyde, M. L., Hutton, D. V., Rathgeber, R. A., & Balch, O. K. (1997). Interrelationships between moisture content of the track, dynamic properties of the track and the locomotor forces exerted by galloping horses. *Journal of Equine Veterinary Science*, *17*(1), 35–42. https://doi.org/10.1016/S0737-0806(97)80456-X

Ratzlaff, M. H., Wilson, P. D., Hutton, D. V., & Slinker, B. K. (2005). Relationships between hoof-acceleration patterns of galloping horses and dynamic properties of the track. *American Journal of Veterinary Research*, *66*(4), 589–595. https://doi.org/10.2460/ajvr.2005.66.589

Roepstorff, L., Johnston, C., & Drevemo, S. (1999). The effect of shoeing on kinetics and kinematics during the stance phase. *Equine Veterinary Journal*, *31*(S30), 279–285. https://doi.org/10.1111/j.2042-3306.1999.tb05235.x

Rogers, C. W., & Back, W. (2003). Wedge and Eggbar Shoes Change the Pressure Distribution under the Hoof of the Forelimb in the Square Standing Horse. *Journal of Equine Veterinary Science*, *23*(7),

306–309. https://doi.org/10.1016/s0737-0806(03)01009-8

Rogers, C. W., & Back, W. (2007). The effect of plain, eggbar and 6°-wedge shoes on the distribution of pressure under the hoof of horses at the walk. *New Zealand Veterinary Journal*, *55*(3), 120–124. https://doi.org/10.1080/00480169.2007.36753

Serra Bragança, F. M., Rhodin, M., & van Weeren, P. R. (2018). On the brink of daily clinical application of objective gait analysis: What evidence do we have so far from studies using an induced lameness model? In *Veterinary Journal* (Vol. 234, pp. 11–23). Bailliere Tindall Ltd. https://doi.org/10.1016/j.tvjl.2018.01.006

Setterbo, J. J., Garcia, T. C., Campbell, I. P., Reese, J. L., Morgan, J. M., Kim, S. Y., Hubbard, M., & Stover, S. M. (2009). Hoof accelerations and ground reaction forces of Thoroughbred racehorses measured on dirt, synthetic, and turf track surfaces. *American Journal of Veterinary Research*, *70*(10), 1220–1229. https://doi.org/10.2460/ajvr.70.10.1220

Singleton, W. H., Clayton, H. M., Lanovaz, J. L., & Prades, M. (2003). Effects of shoeing on forelimb swing phase kinetics of trotting horses. *Veterinary and Comparative Orthopaedics and Traumatology*, *16*(1), 16–20. https://doi.org/10.1055/s-0038-1632749

Sleutjens, J., Serra Bragança, F. M., van Empelen, M. W., ten Have, R. E., de Zwaan, J., Roelfsema, E., Oosterlinck, M., & Back, W. (2018). Mouldable, thermoplastic, glue-on frog-supportive shoes change hoof kinetics in normal and obese Shetland ponies. *Equine Veterinary Journal*, *50*(5), 684–689. https://doi.org/10.1111/EVJ.12814/FORMAT/PDF

Thomason, J. J., & Peterson, M. L. (2008). Biomechanical and Mechanical Investigations of the Hoof-Track Interface in Racing Horses. In *Veterinary Clinics of North America - Equine Practice* (Vol. 24, Issue 1, pp. 53–77). Elsevier. https://doi.org/10.1016/j.cveq.2007.11.007

Trotter, G. W. (2004). Hoof balance in equine lameness. *Journal of Equine Veterinary Science*, *24*(11),

494–495. https://doi.org/10.1016/j.jevs.2004.10.009

van Heel, M. C., Barneveld, van Weeren, P. R., & Back. (2004). Dynamic pressure measurements for the detailed study of hoof balance: The effect of trimming. *Equine Veterinary Journal*, *36*(8), 778–782. https://doi.org/10.2746/0425164044847993

van Heel, M. C., Moleman, M., Barneveld, A., Van Weeren, P. R., & Back, W. (2005). Changes in location of centre of pressure and hoof-unrollment pattern in relation to an 8-week shoeing interval in the horse. *Equine Veterinary Journal*, *37*(6), 536–540. https://doi.org/10.2746/042516405775314925

Weishaupt, M. A., Hogg, H. P., Wiestner, T., Denoth, J., Stüssi, E., & Auer, J. A. (2002). Instrumented treadmill for measuring vertical ground reaction forces in horses. *American Journal of Veterinary Research*, *63*(4), 520–527. https://doi.org/10.2460/ajvr.2002.63.520

Wiggers, N., Nauwelaerts, S. L. P., Hobbs, S. J., Bool, S., Wolschrijn, C. F., & Back, W. (2015). Functional Locomotor Consequences of Uneven Forefeet for Trot Symmetry in Individual Riding Horses. *PLOS ONE*, *10*(2), e0114836. https://doi.org/10.1371/journal.pone.0114836

Willemen, M. A. (1997). *Horseshoeing, a biomechanical analysis*. [s.n.].

Willemen, M. A., Savelberg, H. H. C. M., & Barneveld, A. (1997). The improvement of the gait quality of sound trotting warmblood horses by normal shoeing and its effect on the load on the lower forelimb. *Livestock Production Science*, *52*(2), 145–153. https://doi.org/10.1016/S0301-6226(97)00130-9

Willemen, M. A., Savelberg, H. H. C. M., & Barneveld, A. (1999). The effect of orthopaedic shoeing on the force exerted by the deep digital flexor tendon on the navicular bone in horses. *Equine Veterinary Journal*, *31*(1), 25–30. https://doi.org/10.1111/j.2042-3306.1999.tb03787.x

IV. Appendix

Horse	Year of birth	Age at the study (in years)	Weight (in kilograms)	Height (in cm)	Breed
H1	2006	15	532	161	KWPN Tuigpaard
H2	2006	15	616	160	Friesian Horse
H3	2009	12	608	165	KWPN Rijpaard
H4	2008	13	626	164	KWPN Rijpaard
H5	2011	10	554	159	KWPN Tuigpaard
H6	2007	14	547	154	Irish Piebald & SkewbalI

Table 11: information on the horses used in this research project.

Horse	Toe angle at the steel shoe cycle in degrees (◦) before application of the shoe		Toe angle at the steel shoe cycle in degrees (◦) after removal of the shoe		Toe angle at the tailormade 3D-printed shoe cycle in degrees (◦) before application of the shoe		Toe angle at the tailormade 3D-printed shoe cycle in degrees (◦) after removal of the shoe	
	Left hoof	Right hoof	Left hoof	Right hoof	Left hoof	Right hoof	Left hoof	Right hoof
H1	63.4	62.6	62.4	62.4	58.0	60.0	55.8	57.1
H2	65.0	65.0	65.1	64.6	58.8	60.8	58.5	58.1
H3	63.1	61.1	62.0	60.0	NA	60.2	59.6	57.0
H4	64.0	63.5	61.9	61.7	64.0	63.9	60.7	61.3
H5	61.4	60.1	58.6	58.0	60.3	58.2	59.0	57.9
H6	60.8	61.6	58.8	59.1	60.0	60.6	59.4	59.0
Average (Absolute mean ± SD)	63.0 ± 1.6	62.3 ± 1.8	61.5 ± 2.4	61.0 ± 2.4	60.2 ± 2.3	60.6 ± 1.9	58.8 ± 1.7	58.4 ± 1.6

Table 12: the toe angle before application and after removal of the horseshoe per shoeing condition and per hoof measured by the farriers.

Horse	**Toe angle change at the steel shoe cycle in degrees (◦)**		**Toe angle change at the tailormade 3D-printed shoe cycle in degrees (◦)**	
	Left hoof	Right hoof	Left hoof	Right hoof
H1	-1.0	-0.2	-2.2	-2.9
H2	+0.1	-0.4	-0.3	-2.7
H3	-1.1	-1.1	NA	-3.2
H4	-2.1	-1.8	-3.3	-2.6
H5	-2.8	-2.1	-1.3	-0.3
H6	-2.0	-2.5	-0.6	-1.6
Average (Absolute mean ± SD)	-1.5 ± 1.0	-1.4 ± 0.9	-1.5 ± 1.2	-2.2 ± 1.1

Table 13: toe angle change (decrease (-) or increase (+)), measured by the farriers, per shoeing condition.

Condition	Day	Hoof Width	Inner wall length	Outer wall length	Inner wall angle	Outer wall angle	Hoof length	Heel length	Toe length	Heel angle	Toe angle
Steel	0	10.74 ± 0.03	5.40 ± 0.07	5.52 ± 0.16	76.30 ± 0.33	73.20 ± 0.29	9.37 ± 0.02	4.70 ± 0.08	6.32 ± 0.18	50.64 ± 0.19	64.29 ± 0.26
Steel	46	10.97 ± 0.04	5.89 ± 0.11	5.96 ± 0.15	75.63 ± 0.25	72.48 ± 0.32	9.61 ± 0.10	4.99 ± 0.09	6,70 ± 0.13	52.11 ± 0.73	62.71 ± 0.22
Plastic	0	10.81 ± 0.04	5.30 ± 0.04	5.36 ± 0.03	73.01 ± 0.43	71.46 ± 0.43	9.93 ± 0.07	4.40 ± 0.09	5.95 ± 0.05	55.02 ± 1.45	62.00 ± 0.62
Plastic	46	11.01 ± 0.02	5.50 ± 0.05	5.63 ± 0.04	73.89 ± 0.28	71.03 ± 0.25	10.01 ± 0.11	5.31 ± 0.09	6.75 ± 0.07	56.88 ± 0.79	60.47 ± 0.48

Table 14: hoof conformation changes per shoeing cycle of the left hoof of horse 1.

Condition	Day	Hoof Width	Inner wall length	Outer wall length	Inner wall angle	Outer wall angle	Hoof length	Heel length	Toe length	Heel angle	Toe angle
Steel	0	10.81 ± 0.02	6.20 ± 0.02	6.52 ± 0.11	77.85 ± 0.32	78.28 ± 0.14	10.97 ± 0.13	4.86 ± 0.17	7.49 ± 0.03	53.68 ± 0.46	65.99 ± 0.59
Steel	46	10.97 ± 0.04	5.88 ± 0.05	6.89 ± 0.07	79.07 ± 0.51	74.82 ± 0.47	11.70 ± 0.03	4.98 ± 0.09	8.45 ± 0.20	52.71 ± 1.23	63.45 ± 0.69
Plastic	-3	11.04 ± 0.02	6.20 ± 0.09	6.60 ± 0.05	77.16 ± 0.19	76.14 ± 0.25	11.38 ± 0.03	4.72 ± 0.13	7.50 ± 0.12	55.01 ± 0.76	66.05 ± 0.39
Plastic	46	11.15 ± 0.03	6.50 ± 0.10	6.69 ± 0.07	74.75 ± 0.29	77.48 ± 0.44	11.73 ± 0.05	4.58 ± 0.06	7.80 ± 0.04	51,71 ± 0.64	62.06 ± 0.22

Table 15: hoof conformation changes per shoeing cycle of the right hoof of horse 2.

Condition	Day	Hoof Width	Inner wall length	Outer wall length	Inner wall angle	Outer wall angle	Hoof length	Heel length	Toe length	Heel angle	Toe angle
Steel	0	10.08 ± 0.02	5.94 ± 0.03	6.25 ± 0.03	82.37 ± 0.24	73.04 ± 0.25	10.20 ± 0.02	4.24 ± 0.02	7.50 ± 0.09	54.24 ± 0.71	64.17 ± 0.46
Steel	48	10.22 ± 0.03	6.44 ± 0.05	6.49 ± 0.05	79.53 ± 0.20	74.91 ± 0.28	10.81 ± 0.05	4.70 ± 0.12	7.75 ± 0.04	58.78 ± 0.31	62.61 ± 0.42
Plastic	0	10.22 ± 0.04	5.74 ± 0.08	6.08 ± 0.03	82.36 ± 0.77	72.89 ± 0.45	10.63 ± 0.07	3.88 ± 0.08	6.54 ± 0.05	60.91 ± 0.59	64.87 ± 0.12
Plastic	45	10.28 ± 0.05	5.79 ± 0.05	6.18 ± 0.05	81.04 ± 0.71	72.91 ± 0.53	10.30 ± 0.05	4.38 ± 0.05	7.61 ± 0.07	55.35 ± 0.42	64.11 ± 0.26

Table 16: hoof conformation changes per shoeing cycle of the left hoof of horse 3.

Condition	Day	Hoof Width	Inner wall length	Outer wall length	Inner wall angle	Outer wall angle	Hoof length	Heel length	Toe length	Heel angle	Toe angle
Steel	0	10.94 ± 0.03	5.80 ± 0.02	6.05 ± 0.07	75.58 ± 0.35	70.59 ± 0.48	9.06 ± 0.02	4.90 ± 0.09	6.80 ± 0.07	50.22 ± 0.51	65.44 ± 0.18
Steel	48	10.98 ± 0.04	5.79 ± 0.03	6.08 ± 0.04	75.19 ± 0.33	70.22 ± 0.33	9.83 ± 0.24	4.51 ± 0.07	6.87 ± 0.02	49.84 ± 1.88	62.53 ± 0.44
Plastic	0	10.79 ± 0.01	5.55 ± 0.03	5.44 ± 0.02	75.47 ± 0.11	71.09 ± 0.14	9.86 ± 0.26	4.08 ± 0.23	6.26 ± 0.03	53.99 ± 1.22	65.29 ± 0.66
Plastic	45	11.02 ± 0.01	6.23 ± 0.03	6.12 ± 0.03	72.97 ± 0.31	73.24 ± 0.04	9.46 ± 0.28	5.00 ± 0.23	7.15 ± 0.15	52.50 ± 0.61	62.60 ± 0.59

Table 17: hoof conformation changes per shoeing cycle of the left hoof of horse 4.

Condition	Day	Hoof Width	Inner wall length	Outer wall length	Inner wall angle	Outer wall angle	Hoof length	Heel length	Toe length	Heel angle	Toe angle
Steel	0	11.39 ± 0.01	5.55 ± 0.05	5.56 ± 0.06	69.19 ± 0.62	71.83 ± 0.25	10.35 ± 0.15	4.41 ± 0.15	6.91 ± 0.03	53.20 ± 0.91	59.89 ± 0.98
Steel	45	11.56 ± 0.05	5.48 ± 0.04	5.65 ± 0.07	69.48 ± 0.51	72.84 ± 0.17	10.46 ± 0.08	5.18 ± 0.07	7.23 ± 0.07	54.08 ± 0.34	59.12 ± 0.35
Plastic	0	11.21 ± 0.04	5.19 ± 0.10	5.29 ± 0.08	71.52 ± 0.43	73.28 ± 0.32	9.78 ± 0.39	4.65 ± 0.40	6.57 ± 0.11	49.14 ± 1.29	61.64 ± 0.83
Plastic	48	11.43 ± 0.02	5.84 ± 0.06	5.72 ± 0.05	70.66 ± 0.11	71.69 ± 0.58	9.83 ± 0.27	5.59 ± 0.16	7.60 ± 0.06	47.56 ± 0.87	59.10 ± 0.65

Table 18: hoof conformation changes per shoeing cycle of the right hoof of horse 5.

Condition	Day	Hoof Width	Inner wall length	Outer wall length	Inner wall angle	Outer wall angle	Hoof length	Heel length	Toe length	Heel angle	Toe angle
Steel	0	10.53 ± 0.03	5.35 ± 0.04	5.23 ± 0.04	69.72 ± 0.37	78.38 ± 0.34	10.12 ± 0.28	4.20 ± 0.29	6.72 ± 0.09	46.66 ± 1.48	61.39 ± 0.56
Steel	45	10.82 ± 0.02	5.98 ± 0.05	5.76 ± 0.14	68.57 ± 0.19	78.64 ± 0.18	10.67 ± 0.05	4.65 ± 0.13	6.79 ± 0.14	51.70 ± 0.51	58.43 ± 0.16
Plastic	0	10.50 ± 0.02	5.32 ± 0.04	5.25 ± 0.10	67.75 ± 0.65	77.99 ± 0.26	9.89 ± 0.06	3.88 ± 0.05	6.31 ± 0.11	44.36 ± 0.49	62.91 ± 0.26
Plastic	48	10.95 ± 0.05	5.57 ± 0.06	5.75 ± 0.12	68.73 ± 0.58	75.99 ± 0.31	10.29 ± 0.16	5.00 ± 0.20	6.73 ± 0.10	51.21 ± 0.77	62.75 ± 0.38

Table 19: hoof conformation changes per shoeing cycle of the right hoof of horse 6.

Horse	**Weight steel shoe cycle in grams (g) before application of the shoe**		**Weight steel shoe cycle in grams (g) after removal of the shoe**		**Weight tailormade 3D-printed shoes cycle in grams (g) before application of the shoe**		**Weight tailormade 3D-printed shoes cycle in grams (g) after removal of the shoe**	
	Left hoof	Right hoof	Left hoof	Right hoof	Left hoof	Right hoof	Left hoof	Right hoof
H1	446.2	432.1	424.0	408.2	258.7	232.6	NA [277.5*]	NA [246.0*]
H2	656.9	650.8	618.6	605.1	256.6	269.5	NA [242.4*]	NA [243.2*]
H3	435.7	435.4	412.2	414.8	223.8	212.5	196.2•	182.3•
H4	427.6	422.3	372.7	367.3	204.0	202.1	154.3•	154.9•
H5	439.0	439.8	406.3	406.8	217.3	218.1	195.7•	198.6•
H6	438.7	440.0	389.0	394.4	198.1	198.5	137.6•	152.3•
Average (Mean ± SD)	474.0 ± 89.8	470.1 ± 88.8	437.1 ± 90.7	432.7 ± 86.1	226.4 ± 25.9	222.2 ± 26.1	171.0 ± 29.7	172.0 ± 22.3

*Table 20: weights of the horseshoes before application and after removal of the horseshoe per shoeing condition. * = glue could not be removed or only a small part could be removed. • = glue is mostly removed; little residue is still present.*

Horse	Region	Wear distribution of the left front hoof in the steel shoeing cycle	Wear distribution of the right front hoof in the steel shoeing cycle	Wear distribution of the left front hoof in the tailormade 3D-printed shoeing cycle	Wear distribution of the right front hoof in the tailormade 3D-printed shoeing cycle
H1	Medial heel	I	I	II	II
H1	Lateral heel	II	I	III	II
H1	Medial toe	II	II	I	II
H1	Lateral toe	III	III	III	III
H2	Medial heel	I	I	II	II
H2	Lateral heel	III	III	III	III
H2	Medial toe	III	II	III	III
H2	Lateral toe	IV	IV	III	III
H3	Medial heel	I	I	I	I
H3	Lateral heel	II	II	II	II
H3	Medial toe	II	II	I	II
H3	Lateral toe	III	III	I	III
H4	Medial heel	I	I	II	I
H4	Lateral heel	IV	II	III	III
H4	Medial toe	III	II	II	II
H4	Lateral toe	IV	III	IV	IV
H5	Medial heel	I	I	I	I
H5	Lateral heel	II	II	III	III
H5	Medial toe	II	III	II	II
H5	Lateral toe	III	III	II	II
H6	Medial heel	I	II	III	III
H6	Lateral heel	II	III	IV	IV
H6	Medial toe	II	III	V	IV
H6	Lateral toe	III	IV	V	IV

Table 21: wear distribution per hoof region, expressed with the scale mentioned in Data analysis, per shoeing condition.

V. Supplement

In this section background information about the anatomical planes and rotations, gait biomechanics, kinetics, biomechanics of the hoof, and horseshoes will be given.

Anatomical planes and rotations

In biomechanics, segments movements are described in relationship to other segments. The body of the horse translates in three two-dimensional planes called the sagittal, dorsal and transverse plane, as seen in figure 16 on the left. The segments rotate around three axes: the longitudinal, transverse and vertical rotation axes, illustrated in figure 16 on the right (Clayton & Hobbs, 2017).

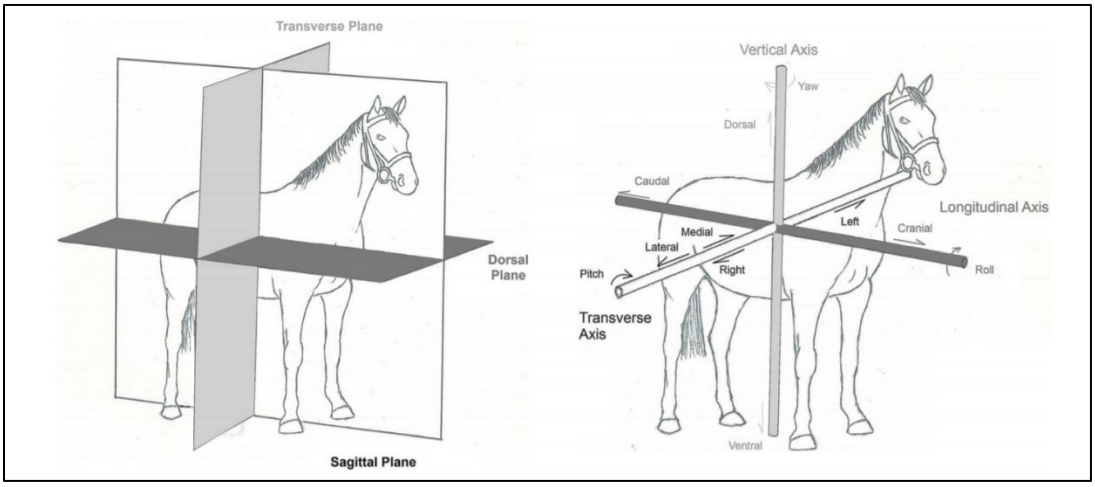

Figure 16: the anatomical planes and rotations axis of the horse (Clayton & Hobbs, 2017).

1. Gait biomechanics

Gaits

The horse has three main gaits: walk, trot and canter, the first being the slowest and the latter being the fastest. Two types of gaits can be distinguished by the symmetry or asymmetry of the hoof landing pattern where symmetric gaits are walk and trot and an asymmetric gait is canter (Leach et al., 1984). Symmetric gaits, such as walk and trot, are most suitable to detect asymmetry, irregularity, or lameness (Baxter et al., 2020).

Walk has a four-beat rhythm where one limb moves after the other. At least two limbs are in contact with the ground, illustrated in figure 17A. Trot is a diagonal gait with a two-beat rhythm in which strides are split by an aerial or suspension phase. During ground contact, diagonal limbs are supporting the body mass, as seen in figure 17B. Canter has a three-beat rhythm and knows an aerial or suspension phase as well. Just after (respectively before) the suspension phase, only the trailing hindlimb (respectively leading forelimb) is supporting the mass of the horse, illustrated in figure 17C1 (Barrey, 2013).

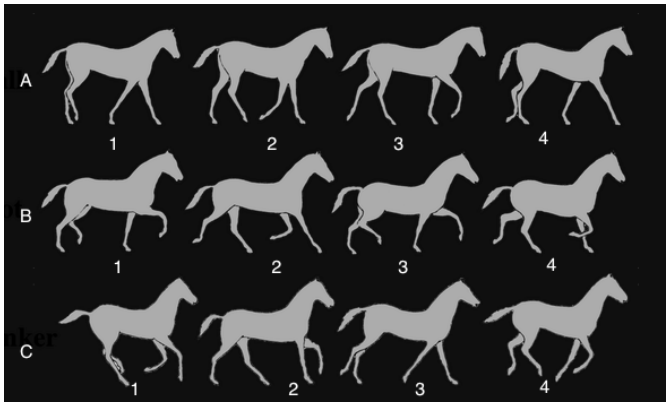

Figure 17: the three main gaits of the horse. A) Walk, B) Trot, C) Canter (www.room2rideinc.com).

Phases of gait cycle

Efforts to make a standard terminology for the description and analysis of equine locomotion were made by various researchers and veterinarians (Clayton, 1989; Leach, 1993; Leach et al., 1984). For the clarity of this paper, the following terms have been defined.

Each stride consists of a phase where the hoof is in contact with the ground, the stance phase, and a phase where the hoof is not in contact with the ground, the swing phase. The stance phase can be divided into three main phases: a deceleration phase, a mid-stance phase and a propulsion phase (Leach, 1993). The deceleration phase, seen in figure 18A and B, starts with initial contact of the hoof with the ground and lasts until the mid-stance, illustrated in figure 18C. The midstance was defined by Drevemo et al. (1980) as the moment where the metacarpus, also known as the canon bone, is in a vertical position in the forelimb (Drevemo et al., 1980). The time between mid-stance and hoof off is known as the propulsion phase, as seen in figure 18D and E. The swing phase is used to describe the phase where the hoof is not in contact with the ground (Barnes & Pinder, 1974; Björck, 1958; Drevemo et al., 1980; Jeffcott et al., 1982; Pratt & O'Connor, 1976).

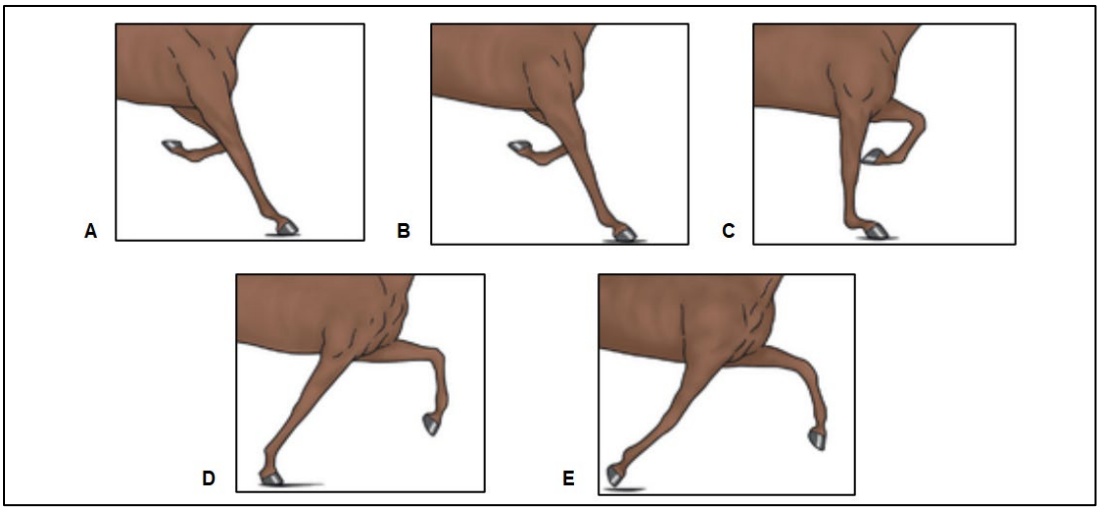

Figure 18: the three phases of stance phase. A and B; deceleration phase, C; mid-stance, D and E; propulsion phase (Fredricson et al., 1972).

2. Kinetics

In kinetic analysis, forces of the movement are looked at. During the stance phase of a stride, the hooves push against the ground generating the ground reaction force (GRF) and propulsion. The GRF and the resulting movement of the horse's limb and body can be described by Newton's laws of Motion. Briefly stated, a force causes or tends to cause a movement, through an equal (reaction) force in the opposite direction, with a speed and direction of movement determined by the magnitude and direction of the (reaction) force (Clayton, 2016).

The horse exerts a force through contact of the hoof with the ground, which is balanced by a force, the GRF, acting against the hoof with the same magnitude but in the opposite direction. The magnitude and direction of the GRF determine the amount and direction of the resulting movement of the body (Clayton & Hobbs, 2019).

The GRF can be decomposed in an orthogonal coordinate system into three components, illustrated in figure 19 (Leach, 1993); the vertical force in the vertical direction (F_z), the longitudinal force in the cranio-caudal direction (F_y) and the transverse force in the medio-lateral direction (F_x) (Clayton, 2016; Oosterlinck et al., 2007). These forces can be normalised by the horse's body mass and are expressed in Newton per kilogram (N/kg). The normalisation of the forces makes comparison between horses with different sizes and weights possible (Clayton & Hobbs, 2019).

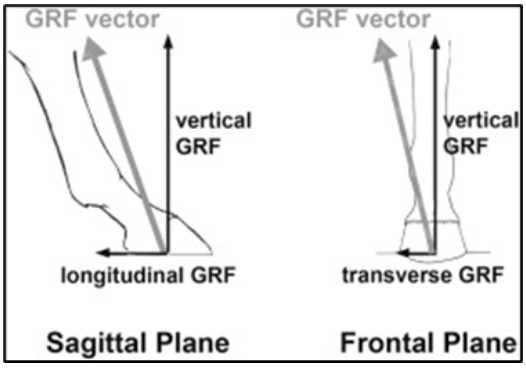

Figure 19: the GRF vector decomposed in three components (Clayton, 2016).

Measuring tools

Kinetic analysis can be conducted with the help of varying instruments such as pressure shoes, force shoes, strain gauges, force plates and pressure plates. Only the force plate and pressure plate will be described in this paper as the research project obtained data from these instruments.

Force plate

Stationary force plates are still the golden standard for kinetic gait analysis and detection of (weightbearing) lameness (Bertrone, 2003; Clayton, 2016; Serra Bragança et al., 2018). A force plate (FP) is a metal plate with piezoelectric sensors around the corners. The system should be embedded in concrete to minimise surrounding vibrations' influence on the measured signals. The runway and plate are covered by non-slip material such as a rubber mat to avoid slipping of the hoof and changes in movement-pattern as the horses will not be able to see the plate (Oosterlinck et al., 2007). A force plate can detect the force amplitude and orientation, the coordinates of the point of application of the force and the moment value of this point (Barrey, 1999). Force plates are precise and accurate measuring tools however, the sensitive surface of a FP is rather small (about 0,5 m^2) and they only record one stance (and sometimes only one limb) at a time (Barrey, 1999; Oosterlinck et al., 2007). Moreover, the installation

requirement and the fact that the system can be costly, make that force plates are not commonly found outside laboratorial environment (Oosterlinck et al., 2010). In 2002, a treadmill was instrumented with FP sensors to overcome the limitations of the stationary FP but is still only available in one specialised lab in Switzerland. Furthermore, the treadmill instrumented with FP sensors can only measure the vertical force (Weishaupt et al., 2002).

Pressure plate

A pressure plate (PP) has a high density of sensors throughout the whole plate (van Heel et al., 2004) and measures consecutive strides (if the size of the plate allows this) (Serra Bragança et al., 2018). Pressure distribution of different regions of the hoof can be obtained during a complete stance phase with a PP. Pressure plates can be dynamically calibrated with the help of simultaneous FP measurements. For this calibration, the PP needs to be on top of the FP (van Heel et al., 2004).

The sensors of a PP are not able to decompose the GRF in three components and the outcome will partly be influenced by shear forces. Furthermore, the force plates that use piezoelectric sensors are more accurate and precise than the pressure plates sensors (Serra Bragança et al., 2018). A study performed by Oosterlinck et al. (2012) with a PP on top of the FP, illustrated in figure 20, showed a high accuracy of the PP compared to the FP during the support phase (mid-stance), a lower accuracy is seen in the impact and break-over phase (deceleration and propulsion phases respectively). The stand-alone PP cannot replace a FP when high accuracy of forces is needed (Oosterlinck et al., 2012).

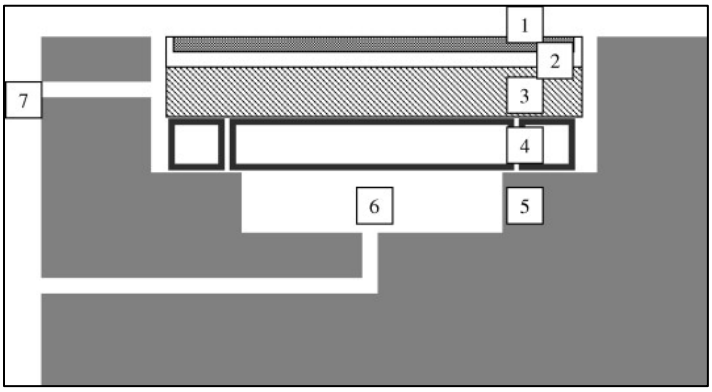

Figure 20: transverse section of the construction used in the study of Oosterlinck et al. (2012) 1: pressure plate; 2: aluminium plate interspaced between pressure plate and force plate; 3: force plate; 4: steel mounting frame of the force plate; 5: concrete foundation; 6: drain; 7: cable channel (Oosterlinck et al., 2012).

Ground reaction force in the stance phase

As described above, the GRF is divided into three components which are typically plotted as force-time graphs, as seen in figure 21. The vertical GRF is a positive force in the upward direction. The force-time curve may show some spiking at the initial hoof impact in the deceleration phase and will then rise to a double (walk) or single (trot, canter) peak before declining to zero at hoof-off. The vertical force peak varies with body mass, limb, gait and speed (Clayton & Hobbs, 2019).

The longitudinal GRF is substantially smaller than the vertical GRF (figure 21). The longitudinal force starts as a negative force directed backward (caudally) due to the deceleration or braking of the forward movement. Around the mid-stance, the longitudinal GRF becomes a positive force directed forward as propulsion starts. After the initial impact, the limb starts to load, and the frictional force increases to decelerate the forward movement of the hoof. Impact spikes in the deceleration phase are more prominent in the longitudinal force than in the vertical force (Clayton & Hobbs, 2019).

The transverse GRF is small when the horse is moving on a straight line (figure 21), as there is no to little influence of the centrifugal force on the locomotion of the horse on the straight line. The transverse force is a positive force when directed medially, which is the case in walk. However, in faster gaits, the transverse force is far more variable (Clayton & Hobbs, 2019).

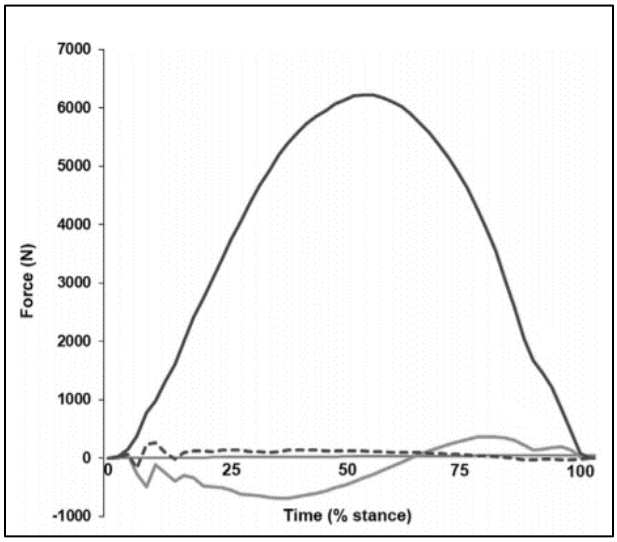

Figure 21: the vertical GRF (dark line), longitudinal GRF (light line) and transverse GRF (dotted line) in trot. Adapted from Clayton, & Hobbs 2019 (Clayton & Hobbs, 2019).

Other kinetic parameters

The stance duration (StDur) is the time in which the hoof is in contact with the ground. In order to compare force-time curves at different speeds, the stance time is normalised to the percentage of stance duration (Clayton & Hobbs, 2019). Important variables concerning the vertical GRF are the peak vertical force (PVF) and vertical impulse (VI), both illustrated in figure 22. The PVF is the maximal amplitude of the vertical force. It corresponds with the peak in the force-time curve of the vertical GRF.

The PVF is proportional to the maximal fetlock extension in the forelimbs (Clayton & Hobbs, 2019). The VI is the summation of the vertical force generated over a period of time and is calculated by the integration of the force-time curve. It corresponds with the area under the curve in the force-time graph, as seen in figure 22. The VI varies with the shape of the vertical GRF curve and the stance duration.

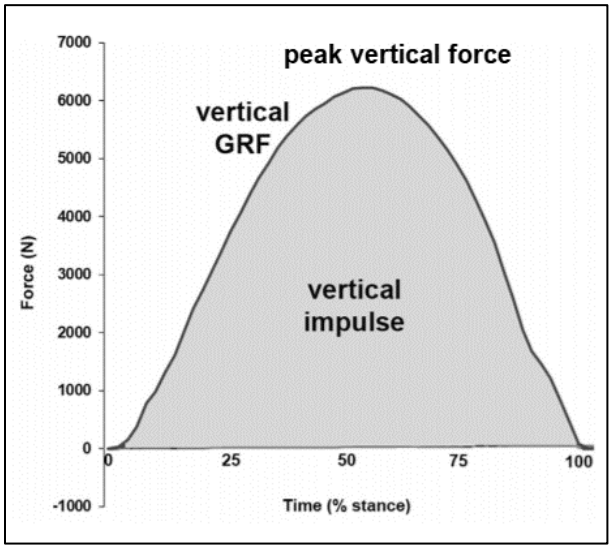

Figure 22: vertical GRF variables; vertical impulse (VI) and peak vertical force (PVF). Adapted from Clayton & Hobbs, 2019 (Clayton & Hobbs, 2019).

Useful variables that describe the longitudinal GRF are peak braking, propulsive forces and time of zero longitudinal force, illustrated in figure 23 (Clayton & Hobbs, 2019). The peak braking force is the highest negative amplitude of the longitudinal GRF. The peak propulsive force is the highest positive amplitude of the longitudinal GRF. Both have corresponding impulses, as seen in Figure 23. The time of zero longitudinal force corresponds with the mid-stance.

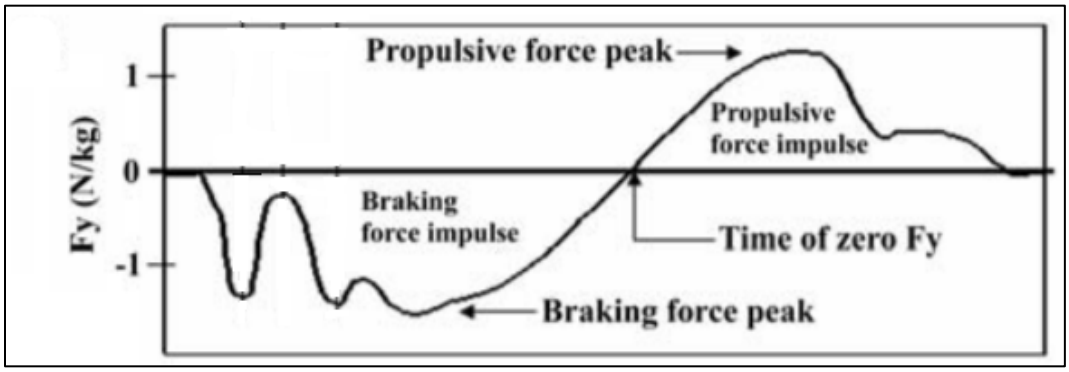

Figure 23: longitudinal GRF variables. Adapted from Clayton 2016 (Clayton, 2016).

The hoof region where the initial contact of the hoof with the ground is, is referred to as the landing orientation. The contact area refers to the area under the hoof that is in contact with the ground. The contact pressure is the pressure exerted on the ground by the hooves of the horse. The contact pressure varies with the contact area and body mass of the horse (Clayton & Hobbs, 2019). The peak contact pressure is the highest pressure measured during the stance phase. The pressure distribution describes the distribution of the pressure over the contact area. The centre of pressure (COP) is the GRF's point of application under the hoof. The COP path tracks the COP for the duration of a stance phase as the pressure distribution changes, as seen in figure 24 (Clayton & Hobbs, 2019).

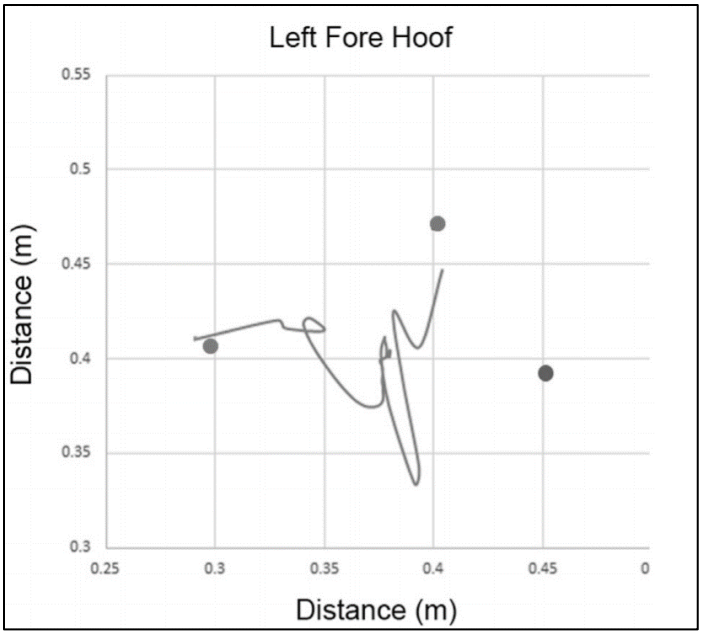

Figure 24: the COP path beneath the left fore hoof of a horse during one stance phase at trot. The dots represent the positions of markers on the distal hoof wall. Initial hoof contact is close to the lateral marker and lift off is close to the dorsal marker in this example (Clayton & Hobbs, 2019).

3. Biomechanics of the hoof

Functional anatomy of the hoof

The important internal and external structures of the hoof are illustrated in figure 25. The hoof capsule includes the coronet, the wall, the sole, the frog and the heels. In barefoot condition the frog, heels and part of the soles are in contact with the ground while the coronet is found in the division between the hoof wall and skin (Back & Pille, 2013). The equine hoof consists of three bones; the coffin bone (distal phalanx), navicular bone (distal sesamoid bone) and part of the short pastern bone (middle phalanx) which all take part in the formation of the distal interphalangeal joint (Kainer, 1989). Two short collateral ligaments arise from each side of the distal end of the short pastern bone and widen before

attaching to the dorsal edges of the cartilage surrounding the coffin bone. The suspensory navicular ligament (the collateral sesamoid ligament) extends from the distal part of the long pastern to the proximal surface of the navicular bone. The interosseous ligament origins at the distal surface of the navicular bone and attaches at the flexor surface of the coffin bone. The deep digital flexor tendon goes around the palmar and plantar side of the navicular bone before attaching to the flexor surface of the coffin bone as well (Kainer, 1989). The coffin bone is surrounded by the medial - and lateral cartilage, these cartilages are connected to the navicular- and short pastern bone by connective tissue. Between the cartilage lies the digital cushion and venous plexus (Back & Pille, 2013).

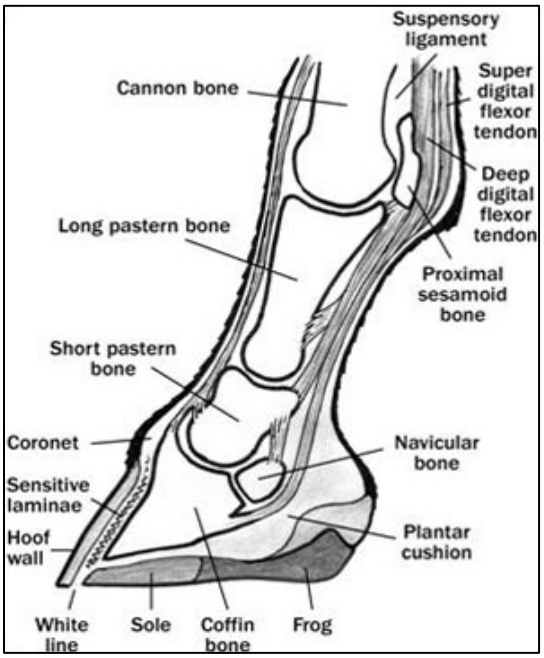

Figure 25: anatomy of the hoof (www.ontario.ca).

Hoof balance

The hoof balance is assessed for trimming, shoeing, lameness exam and health check-ups. Imbalance of the hoof is, empirically, often linked to distal limb lameness in horses (Parks, 2011; Trotter, 2004). As the hoof is a three-dimensional structure, the cranio-caudal and medio-lateral plane should be balanced in the static geometry of the hoof and in the dynamic interaction of the hoof with the surface (Parks, 2011). Hoof balance is traditionally evaluated by visual observations (Oosterlinck et al., 2013; van Heel et al., 2004). However, dynamic abnormalities may not be observed properly by the human eye in gaits faster than walk (Parks, 2011). Over the years, sensitive measurements techniques such as: high frequency cinematography, force plates and pressure plates, gave new insights to the effects of imbalanced and balanced hooves (Clayton, 1990; Crevier-denoix et al., 2001; Oosterlinck et al., 2013; van Heel et al., 2004).

Cranio-caudal balance

The cranio-caudal balance, also known as the toe-heel balance, is examined from a lateral view. The cranio-caudal balance is made of two components: the alignment of the dorsal hoof wall with the pastern axis and alignment of the weightbearing surface of the hoof with the weight bearing axis of the canon bone, illustrated in figure 26 (Back & Pille, 2013).

Medio-lateral balance

The medio-lateral balance is observed in frontal plane. The lengths and angles of the medial and lateral walls of the hoof are determined and modified to achieve balance using two different techniques. The first determines the medio-lateral balance using the static geometry of the limb axis where the ground surface of the hoof wall is aligned perpendicular to the axes of the canon bone and phalanges, as seen in

figure 27. The other technique observes the dynamic interaction of the hoof with the surface through hoof-landing patterns. The hoof is trimmed so that the hooves lands either simultaneously on the medial or lateral heels or flat-footed (Balch et al., 1997). However, visual examination of the dynamic hoof balance is limited by the human eye as described above.

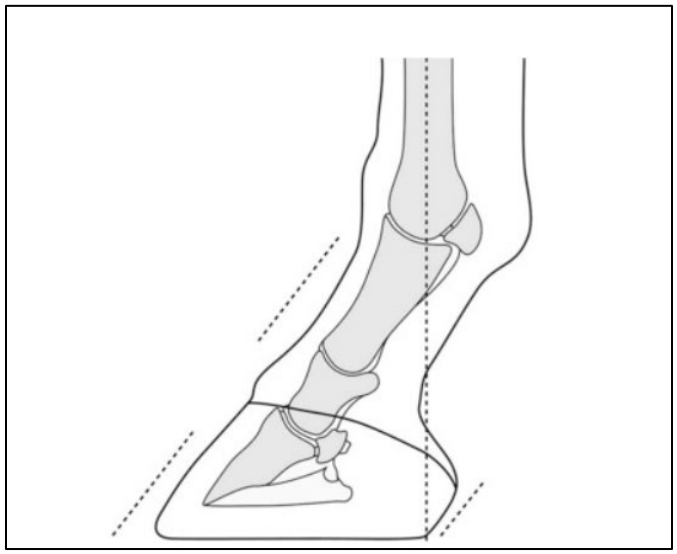

Figure 26: traditional guidelines for the cranio-caudal balance. Alignment dorsal hoof wall with pastern and alignment of the weightbearing axis of the canon bone with the weightbearing surface of the heels (Parks, 2011).

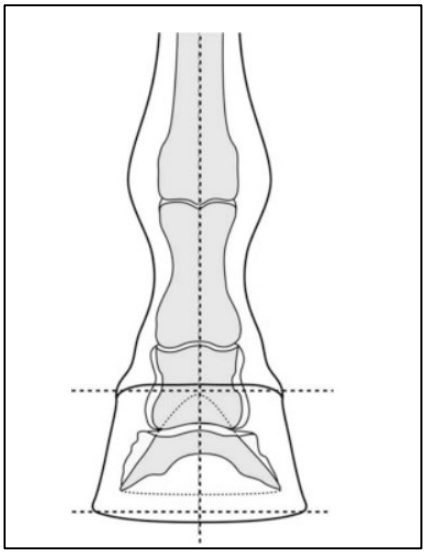

Figure 27: traditional guidelines for the medio-lateral balance. Perpendicular alignment of the hoof wall with the limb axis (Parks, 2011).

Functions of the hoof and the hoof mechanism

Barrey (1990) suggested the following biomechanical functions of the hoof. The caudal region is associated with biomechanical damping function and consists of the next structures and mechanism; the frog, heel expansion, the digital cushion and the venous plexus. The central region is known for its supporting function where the sole and third phalanx form an arch-like structure. The cranial region,

associated with the propulsion function is composed of the toe, sole and coffin bone and has a large contact surface during the propulsion phase (Barrey, 1990).

The hoof mechanism is a result of forces exerted by the horse through the hooves. Forces implied on the coffin bone during locomotion of the horse include tension toward the lamellae of the hoof wall, tension from the deep digital flexor, downward compression from the middle phalanx, upward compression from the soles and forces implied on the extensor process of the suspensory ligament and common digital extensor (Kainer, 1989). From impact in the deceleration phase, the forces mentioned above will cause the following conformation of the hoof. The thinner, more elastic heels will expand and make the quarters flare to the side. This movement is accompanied by a caudoventrally rotation of the proximal dorsal hoof wall and even a slight downward rotation of the coffin bone. This compression of the hoof wall is assumed to cause tension in the lamellae. The sole and frog preform a downward movement, where the frog is known to support the structures of the foot and reduce some strain upon impact. The wedge shape of the frog distributes the forces through the wall and digital cushion (Kainer, 1989). During the locomotion of the horse, the digital cushion and venous plexus are compressed, assisting the venous blood return to the heart (Hoffmann et al., 2001; Pietra et al., 2004). The hoof mechanism phenomenon, as described above, is illustrated in figure 28.

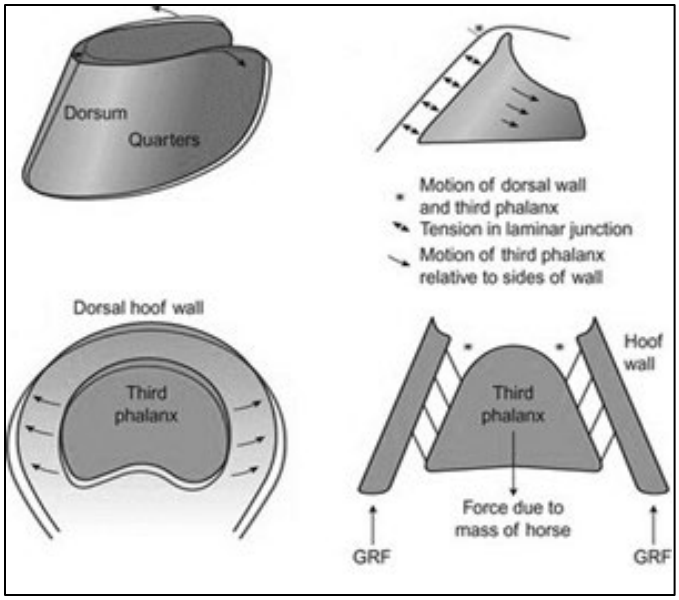

Figure 28: schematic drawing of the hoof mechanism phenomenon. The dark line represents the unloaded hoof wall, the light line shows the change in shape that occurs during weight-bearing. Under load the dorsal wall flattens and moves palmarly, while the heels move laterally and caudally (Douglas, 1996).

Surface interactions

The hoof-ground interaction plays an important role in the kinetics of the hoof. The resistance of the track to the hoof impact and loading of the hoof determine the rate of loading of the limb, and thus the intensity of impact and amplitude of the vertical hoof force (Barrey, 1989; Barrey et al., 1990; Frederick & Henderson, 1970; McMahon & Greene, 1979; Nigg, 1983; Thomason & Peterson, 2008).

The loading of the track can be divided into two components: the vertical component which is related to the hardness of the surface and the horizontal component which is related to the frictional properties of the ground resulting in a shear force. Relevant properties of the surface are the rate-dependent stiffness of the vertical axis during the loading of the limb, and the stiffness and strength of the soil when loaded

in the horizontal plane (Thomason & Peterson, 2008). Several researchers made efforts to describe relevant surface properties (Barrey, 1990; Ratzlaff et al., 1997, 2005; Setterbo et al., 2009).

According to research by Barrey et al. (1990), the damping properties of surface can be divided into three types: no damping (e.g. asphalt), structural damping (e.g. wood) and friction damping (e.g. sand). Structural damping is achieved by deformation of material in contact, while friction damping is achieved by displacement of small particles. During this research, horses were trotted on asphalt, sand, and wood with different property values for dry density, water content and percentage of organic materials. The dry density seemed to influence the peak acceleration (shock) and vibration frequency the most. The shock and vibration were smaller in surfaces with higher water content and higher percentage of organic materials (Barrey et al., 1990).

4. Shoes

The horseshoe was originally developed to protect the hoof from excessive wearing. Nowadays, horseshoes are used to protect the hoof from wearing, improve performance, prevent injuries by adjusting the shoe or adding pads, or as an orthopaedic aid (Willemen et al., 1999). It is important to know the effects of different types of shoes as improper shoeing can cause lameness in horses (Moyer & Anderson, 1975). In the past, the lack of research on different types of shoes was of great concern (Leach & Crawford, 1983). Researchers, farriers, and veterinarians have developed new techniques and methods to evaluate different types of shoes. Some aspects that influence the biomechanics of the horse are the material of the shoe, the weight of the shoe and the shape of the shoe. These aspects will be discussed in the next paragraphs.

Shoe material

Materials have their own properties, such as stiffness/elasticity and wear resistance, which will cause them to interact differently with the hooves and ground surfaces. For example, the shock absorption of aluminium is larger than the shock absorption of steel. And the shock absorption of plastic is larger than the shock absorption of aluminium. The use of visco-elastic soles can increase the shock absorption even more (Oosterlinck et al., 2017).

Benoit et al. (1993) compared damping effects of 16 types of shoeing. The lighter shoes, made of polymer, had a higher shock reduction compared to steel shoes as polymer is less stiff than steel (Benoit et al., 1993).

Iron or steel shoes are more rigid than most shoes, which leads to less deformation of the hoof when strains are applied. This is supported by findings in a study by Brunsting et al. (2019), who found steel shoes limit the heel expansion of the hoof. This restricts the frog from touching the ground yet, the frog is an important shock absorber (Brunsting et al., 2019). A study by Pardoe et al. (2001) mentioned that some horse owners reported that their horses are more comfortable in plastic shoes. This could be explained by the lower braking forces that were found in the plastic shoe or the more graduate rise of the force compared to the regular shoe which results in less jarring of the limb. This corresponds with the findings in a study by Back et al. (2006) who found less friction in plastic shoes compared to steel hoes (Back et al., 2006; Pardoe et al., 2001).

Shoe weight

The effect caused by the weight of horseshoes are more prominent during the swing phase as added weight of the shoes affect the inertia and momentum of the distal limb (Singleton et al., 2003; Willemen et al., 1997). The increased weight of the limb leads to a more animated trot (Willemen et al., 1997). In

research performed on the effects of different types of shoes, the differences in kinetic effects during the swing phase were larger between shod and unshod horses than between the different types of shoes (Singleton et al., 2003; Willemen et al., 1997).

Willemen et al. (1997) described the effect of horseshoes on the load of the distal limb in the stance phase. The GRF was slightly higher in the shod horse however, this result was not significant. This was also found in the research performed by Roepstoff et al. 1999 (Roepstorff et al., 1999; Willemen et al., 1997).

Shoe shape

The shape of the shoe directly influences the contact surface and thus the pressure distribution under the hoof (Hagen et al., 2017; Oosterlinck et al., 2017). By modifying the surface of contact or pressure distribution under the hoof, it has become possible to relieve specific traumatised structures in the limb of the horse. For example, in laminitis an expanded polystyrene sole increases the contact surface, decreases the pressure, and moves the centre of pressure (CoP) backwards to relieve the strains on the navicular bone (Oosterlinck et al., 2017).

Eggbar - and wedge shoes are often used to minimise heel pain in horses with the navicular syndrome. Eggbar shoes have extended branches which connect at the heel, increasing the toe-to-heel axis length. With the increased length, a caudal shift of the centre of pressure was seen. Moreover, the eggbar shoes reduced the peak pressure compared to the regular shoe implying that the eggbar shoe distributed the weight more than the regular shoe (Rogers & Back, 2003, 2007). Wedge shoes slowly increase in height at the branches to the heel. The wedge shoes did not alter the centre of pressure however, there was a lower overall shoe pressure in the forelimbs implying that there is a reduced loading in the forelimbs (Rogers & Back, 2003, 2007).